Biomaterials Science

ROYAL SOCIETY OF CHEMISTRY

PAPER

View Article Online
View Journal | View Issue

Cite this: *Biomater. Sci.*, 2024, **12**, 4823

Extended siponimod release *via* low-porosity PLGA fibres: a comprehensive three-month *in vitro* evaluation for neovascular ocular diseases†

Rasha A. Alshaikh, [a,b] Krishnakumar Chullipalliyalil,[c] Christian Waeber [a,d] and Katie B. Ryan *[a,e]

Neovascular ocular diseases are among the most common causes of preventable or treatable vision loss. Their management involves lifelong, intravitreal injections of anti-vascular endothelial growth factor (VEGF) therapeutics to inhibit neovascularization, the key pathological step in these diseases. Anti-VEGF products approved for ocular administration are expensive biological agents with limited stability and short half-life. Additionally, their therapeutic advantages are hindered by high treatment resistance, poor patient compliance and the need for frequent, invasive administration. Herein, we used electrospinning to develop a unique, non-porous, PLGA implant for the ocular delivery of siponimod to improve ocular neovascular disease management. Siponimod is an FDA-approved drug for multiple sclerosis with a novel indication as a potential ocular angiogenesis inhibitor. The electrospinning conditions were optimised to produce a microfibrous, PLGA matte that was cut and rolled into the desired implant size. Physical characterisation techniques (Raman, PXRD, DSC and FTIR) indicated siponimod was distributed uniformly within the electrospun fibres as a stabilised, amorphous, solid dispersion with a character modifying drug–polymer interaction. Siponimod dispersion and drug–polymer interactions contributed to the formation of smooth fibres, with reduced porous structures. The apparent reduced porosity, coupled with the drug's hydrophobic dispersion, afforded resistance to water penetration. This led to a slow, controlled, Higuchi-type drug diffusion, with ~30% of the siponimod load released over 90 days. The released drug inhibited human retinal microvascular endothelial cell migration and did not affect the cells' metabolic activity at different time points. The electrospun implant was physically stable after incubation under stress conditions for three months. This novel siponimod intravitreal implant broadens the therapeutic possibilities for neovascular ocular diseases, representing a potential alternative to biological, anti-VEGF treatments due to lower financial and stability burdens. Additionally, siponimod interaction with PLGA provides a unique opportunity to sustain the drug release from the electrospun fibres, thereby reducing the frequency of intravitreal injection and improving patient adherence.

Received 6th March 2024,
Accepted 3rd August 2024

DOI: 10.1039/d4bm00339j

rsc.li/biomaterials-science

1. Introduction

Proliferative diabetic retinopathy, neovascular age-related macular degeneration, and retinal vein occlusion are among the leading causes of treatable and preventable blindness globally, with an expected increase in their prevalence due to an ageing population.[1,2] These debilitating diseases are characterised by regional hypoxia and inflammation that trigger neovascularization in the ocular posterior segment. In contrast to typical retinal vessels, neovascular blood vessels show defective intercellular junctions and disrupted endothelial coverage, leading to the leakage of blood and serum into the surrounding tissue, resulting in oedema, haemorrhage and progressive vision loss.[3]

Current management relies on inhibiting vascular endothelial growth factor (VEGF), one of the most crucial, hypoxia-induced, growth factors that triggers neovascularization. The treatment protocol includes the lifelong, repetitive, intravitreal injection of an anti-VEGF therapy, which neutralises VEGF in the vitreous and posterior segment tissues. Currently approved

[a]*School of Pharmacy, University College Cork, Cork, Ireland.*
E-mail: Katie.ryan@ucc.ie; Tel: +353-21-4901680
[b]*Department of Pharmaceutical Technology, Faculty of Pharmacy, Tanta University, Tanta, Egypt*
[c]*Centre for Advanced Photonics & Process Analysis, Munster Technological University Cork, T12 P928 Cork, Ireland*
[d]*Department of Pharmacology and Therapeutics, School of Medicine, University College Cork, Cork, Ireland*
[e]*SSPC The SFI Research Centre for Pharmaceuticals, School of Pharmacy, University College Cork, Cork, Ireland*

† Electronic supplementary information (ESI) available. See DOI: https://doi.org/10.1039/d4bm00339j

anti-VEGF agents are of biological origin[4] and have multiple drawbacks, including a high rate of treatment resistance and low real-life efficacy compared to clinical trials.[5,6] These limitations can be addressed, at least partially, by inhibiting other signalling molecules leading to neovascularization. Faricimab-svoa (VABYSMO®) is a bispecific monoclonal antibody, approved by the FDA in 2022, that binds to VEGF-A and Angiopoietin-2. Clinical trials are underway for RBM-007, an RNA aptamer against basic fibroblast growth factor (bFGF) (NCT04200248, NCT04895293),[7] IBI302, a bispecific fusion protein against VEGF and the complement cascade (NCT04820452, NCT05961007),[8] AR-13503, a Rho kinase and protein kinase C inhibitor (NCT03835884), and sonepcizumab, an antibody against the lipid mediator, sphingosine 1-phosphate (S1P) (NCT00767949, NCT01414153).

Another major challenge with currently approved anti-VEGF therapies lies in their short half-life within the vitreous, thereby requiring recurrent monthly intravitreal injections.[9] Their biological nature also presents cost and stability constraints when designing sustained delivery systems to minimise the frequency of intravitreal injection. Consequently, other clinical trials have explored various small molecules and more stable VEGF signalling inhibitors, including tyrosine kinase inhibitors (TKIs).[10] The small molecule properties help to simplify their formulation into polymeric-drug delivery systems (*e.g.*, microparticles, injectable implants), which can offer sustained drug delivery for 4–6 months (NCT04085341, NCT04989699).

Siponimod, a sphingosine 1-phosphate receptor (S1PR) modulator, is a promising small molecule that inhibits ocular neovascularisation *via* a novel mechanism of action.[11–16] It exerts its actions *via* $S1PR_1$ modulation, inhibiting retinal endothelial cell migration and protecting against endothelial barrier breakdown *in vitro*.[11–15] Subconjunctival administration of siponimod has been shown to prevent the progression of corneal neovascularization in albino rabbits.[15] Siponimod did not show any toxic effects after intravitreal injection in rabbits. However, its intravitreal half-life is very short, <4 h, which necessitates the development of a sustained drug delivery system to maintain therapeutic drug concentrations over an extended period.[17] Considering the novel mechanism of action of siponimod as an angiogenesis inhibitor, coupled with its small molecular weight and non-biological origin, developing a sustained drug delivery system can offer an alternative or additive treatment for ocular neovascular diseases with the added benefit of reduced injection frequency.

Electrospinning is investigated in drug delivery applications due to its ability to produce biocompatible systems with controlled physical properties and tuneable drug delivery rates.[18,19] One of the most common polymers used in electrospinning is PLGA (poly(lactic-*co*-glycolic acid)), a slowly degrading, hydrophobic polymer employed in more than 20 FDA-approved products,[20] including the intravitreal injectable implant Ozurdex® (Allergan, Dublin, Ireland; a dexamethasone implant for macular oedema and uveitis).[4] PLGA is also employed in GB-102, a depot forming microparticle formulation carrying sunitinib maleate, which is currently in phase II clinical trials for multiple ocular neovascular pathologies.[21]

Electrospinning of PLGA is commonly investigated to produce biomimetic fibrous meshes[22] and has been previously studied for ocular applications.[23,24] However, due to the higher porosity and surface area of electrospun matrices, compared to melt-extruded or solvent-casted matrices, their drug release rates tend to be less sustained.[25,26] This has motivated other researchers to employ complicated techniques during electrospinning to achieve the benefit of sustained drug delivery for different therapeutic applications. These techniques include the formation of a drug core in a polymer shell using coaxial electrospinning,[27–29] coating implants with electrospun nanofibres for sustained dual drug release[30] and formation of nanoparticles[31] or nanotubes in electrospun fibres.[32] These techniques were effective in sustaining drug release for up to three months. However, added costs and complexity can limit their scale-up potential.

In this study, we aimed to develop an intravitreal implant to sustain the delivery of siponimod using uniaxial electrospinning, a simple technique with a high probability of scaling up. The drug–polymer interaction between siponimod and PLGA was harnessed to produce distinctively less-porous microfibres that sustain the drug release for a minimum of three months, which could minimise the number of intravitreal injections needed to manage ocular neovascular diseases effectively. The microfibrous PLGA matrix was loaded with a theoretical siponimod content of up to 10.7% w/w. Implant fibre size, siponimod distribution in the fibres, encapsulation efficiency, release and stability were characterised to investigate the feasibility of the implant to control release at therapeutic levels for a minimum of three months. The study also probed the detected interaction between siponimod and the PLGA matrix to explain the relationship between fibre morphology and release properties. The efficacy of the drug released at day 90 was confirmed using retinal endothelial cell migration. Any impact of the released drug and implant degradation products on cell metabolic activity at various times was examined using the Thiazolyl Blue Tetrazolium Bromide (MTT) Assay. The integrity of the implant and the loaded drug under stress conditions were also studied to confirm the suitability of the implant for prolonged intravitreal implantation.

2. Materials and methods

2.1. Materials

Siponimod (BAF312, 516.6 g mol^{-1}) was a kind gift from Novartis Pharma AG, Basel, Switzerland. Resomer RG858 S (poly(lactic-*co*-glycolic acid) 85 : 15 (PLGA 85 : 15); Material no. 99023783) was purchased from Evonik GmbH, Darmstadt, Germany. Dichloromethane (DCM), dimethylformamide (DMF), acetone, ethyl acetate (EA), dimethyl sulfoxide (DMSO) phosphate-buffered saline (PBS), acetonitrile (HPLC grade), water (HPLC grade), phosphoric acid, FBS (Foetal bovine

serum) and PENSTREP® (penicillin–streptomycin) were purchased from Merck, Ireland.

2.2. Preparation of electrospun fibres

PLGA 85 : 15 (Resomer RG858 S) was dissolved in a glass vial at 8% w/w in dichloromethane (DCM). The solutions were stored at 4 °C overnight to ensure complete dissolution. Before electrospinning, they were equilibrated to room temperature for at least one hour. Polymer solutions were then electrospun using the Spraybase® (Spraybase, Ireland) electrospray instrument kit (CAT000002) and an AL-2000 syringe pump (World Precision Instruments, USA). The solutions were pumped at a flow rate of 0.7 mL h^{-1} through connecting tubing (1 mm diameter) to an emitter nozzle (0.9 mm diameter), under high voltage maintained at 16 kV. The discharged product was collected on a stainless-steel plate wrapped in aluminium foil and positioned 15 cm from the emitter nozzle. Collected samples were kept in a fume hood overnight to enable complete solvent evaporation before storing the product at 4 °C until use. After optimising polymer concentration and solvent type, these conditions were selected to produce a bead-free, microfibrous matte of PLGA (Fig. S1, S2 and Table S2†).

For siponimod-loaded formulations, siponimod was added to the PLGA solution at different weight ratios before electrospinning. Then, the drug–polymer mixture was sonicated for 10 min to aid drug dissolution before being equilibrated at room temperature for a minimum of 1 h. Siponimod weight ratios relative to PLGA weight (Si : PLGA) were 0.5 : 100, 4 : 100 and 8 : 100. Additionally, a formulation with higher siponimod content of 12 : 100 relative to PLGA weight was also prepared as siponimod content was below the detection limit for solid-state characterisation techniques using lower weight ratios. These formulations are abbreviated as Si : PLGA (n : 100), where n refers to the number of weight parts of siponimod to 100 weight parts of PLGA. For example, Si : PLGA (8 : 100) is a formulation loaded with 8 weight parts of siponimod to 100 weight parts of PLGA. This represents 8 weight parts of siponimod to 108 weight parts of the formulation, corresponding to a theoretical drug content of 7.4% w/w. The details of the prepared formulations are summarised in Table 1.

2.3. Morphology and size distribution of PLGA microfibres

The morphology of the electrospun microfibres was observed by scanning electron microscopy (SEM). Samples were mounted on stubs using double-sided carbon tape before being sputter-coated with a 5 nm thick coat of gold–palladium (80 : 20). Images were captured using a JEOL JSM-5510 microscope (Jeol Ltd, Tokyo, Japan) at a standard working distance of 22–23 mm and accelerating voltage of 5 kV. For each formulation, three different samples were examined using SEM, and at least 5 random micrographs were captured for each sample. The captured images were analysed using ImageJ® software to calculate the diameter of electrospun fibres. In each micrograph, the diameter of a minimum of 15 fibres was recorded. These measurements (a minimum of 225 per formulation) were used to calculate the mean fibre diameter and construct the size distribution graph.

Table 1 Summary of the electrospun formulations' characteristics including composition, codes, drug content, encapsulation efficiency, mean fibre diameter and surface morphology

PLGA 85 : 15 weight (mg)	Siponimod weight (mg)	Formulation code showing weight ratios	Theoretical drug content[a] (%w/w)	Practical drug content[b] (%w/w)	Encapsulation efficiency[c] (%)	Mean fibre diameter[d] (μm)	Fibres' surface morphology
100	0	ES PLGA	0	N/A	N/A	1.85 ± 0.81	Porous ~200 nm pores
100	0.5	Si : PLGA (0.5 : 100)	0.5	0.43 ± 0.16	85.48 ± 8.90	1.57 ± 0.78	Porous ~200 nm pores
100	4	Si : PLGA (4 : 100)	3.85	2.99 ± 0.29	77.68 ± 7.50	1.92 ± 1.09	Non-porous
100	8	Si : PLGA (8 : 100)	7.41	6.09 ± 0.46	82.17 ± 6.14	1.86 ± 0.80	Non-porous
100	12	Si : PLGA (12 : 100)	10.7	9.07 ± 0.52	84.59 ± 4.91	1.62 ± 0.74	Non-porous

[a] Theoretical drug content was calculated based on the amount of siponimod used to prepare each formulation. [b] Practical drug content is the actual amount of siponimod in the prepared formulation analysed using HPLC post-production. [c] The encapsulation efficiency of the electrospun samples was determined by the established HPLC method. The values represent the mean ± standard deviation (n = 3). [d] Values are presented as the mean of 225 fibre measurements ± standard deviation.

2.4. Physical characterisation of the electrospun product

2.4.1. Differential scanning calorimetry (DSC). The thermal behaviour of the electrospun fibres and their unprocessed components was investigated using a TA Q1000 differential scanning calorimeter (TA instruments, USA). A known weight of the material was placed in a hermetically sealed aluminium pan and heated to 380 °C using a ramp rate of 10 °C per minute under a constant flow of nitrogen (flow rate 50.0 mL min^{-1}). Furthermore, the glass transition of amorphous siponimod was determined using the same instrument, by heating the drug sample at 10 °C min^{-1} to 138 °C, then cooling the sample at the same rate to 20 °C before heating the sample for a second heating cycle to 380 °C at 10 °C min^{-1}.

2.4.2. Powder X-ray diffraction (PXRD). The crystalline structures of the unprocessed drug and polymer and the electrospun fibres were investigated using a Stadi MP diffractometer (STOE & Cie GmbH, Darmstadt, Germany) equipped with a Cu X-ray source and a silicon strip detector. The diffractograms were recorded through a two-theta (2θ) range from 3° to 90° at a scanning step size of 2°, and a step time of 90 s. Data acquisition and management were achieved using WinXPOW PowDat software (STOE & Cie GmbH, Darmstadt, Germany).

2.4.3. Fourier transform infrared (FTIR) spectroscopy. FTIR spectroscopy was conducted to investigate the potential interaction between siponimod and PLGA. The FTIR spectra of unprocessed components and electrospun fibres were recorded using the Two™ FTIR Spectrometer equipped with a $LiTaO_3$ detector (PerkinElmer, Massachusetts, USA) with a sensitivity of 0.5 cm^{-1}. The FTIR spectrum of each sample was recorded within the range of 4000–450 cm^{-1} using the average accumulation of 16 scans per sample. Data acquisition and handling were conducted utilising the PerkinElmer Spectrum™ software. Similar experimental settings were used to record the FTIR spectrum of a co-precipitated mixture of siponimod and PLGA 85 : 15. To prepare the co-precipitated sample, equal weight ratios of siponimod and PLGA 85 : 15 were dissolved in DCM (electrospinning solvent), and the solvent was allowed to evaporate at room temperature. Then, the sample was kept in a fume hood overnight to enable complete solvent evaporation before storing the product at 4 °C prior to analysis.

2.4.4. Raman spectroscopy. Unprocessed PLGA, unprocessed siponimod and electrospun fibres were analysed at the Centre for Advanced Photonics and Process Analysis (CAPPA), Munster Technological University (Cork, Ireland) using a Witech Alpha 300R Raman imaging microscope. The parameters used for the analysis are listed in Table S1.† All the measurements were conducted at a non-polarised, visible, excitation wavelength of 633 nm. The spectral region between 1400–1700 cm^{-1} was identified as the region of interest. The characteristic intense vibrational peaks for siponimod and PLGA appeared at 1595 cm^{-1} and 1453 cm^{-1}, respectively. Raman maps were run on this spectral region to identify siponimod's presence and distribution within the electrospun matte. The microfibres were imaged in visible light using the confocal system of a Witech Raman microscope. Raman spectra from individual points were then collected and collated to form a "Raman map" to show the distribution of siponimod in the fibres. Initially, larger area maps with 100 data points (10 × 10 μm, 2.5 μm individual spot size) were collected across different regions on the PLGA scaffolds. This was followed by constructing higher-resolution maps for individual fibres. For maps with higher spatial resolution, the confocal system measured the Raman intensity of an individual fibre at each X–Y point focused on the fibre's surface. A filter was applied to the intensity at 1595 cm^{-1} corresponding to the siponimod vibrational peak and overlapped on the scan area in the visible image to achieve the high-resolution Raman intensity maps.

2.5. High-performance liquid chromatography (HPLC) analysis of siponimod

Siponimod concentration was quantified by HPLC (1260 Infinity chromatographic system, Agilent Technologies, Santa Clara, California) and UV/VIS detection. Briefly, chromatographic separation was achieved using a reverse phase 4.6 × 150 mm Eclipse Plus® column (particle size 5 μm) (Agilent technologies). The mobile phase comprised 45% HPLC-grade water supplemented with 0.01% v/v phosphoric acid, pH = 3.0 ± 0.1 (A) and 55% acetonitrile (B). The mixture was pumped at 1 mL min^{-1}, and the effluent was monitored at 220 nm. Serial dilutions of standard siponimod working solutions over the concentration ranges of 0.5 μg mL^{-1}–10 μg mL^{-1} were prepared in the mobile phase and were used to develop the calibration curve.[33] Unknown siponimod concentrations were determined using the straight-line equation of the average calibration. All unknown samples were analysed in duplicate.

2.6. Drug content and encapsulation efficiency

The practical drug content (% w/w) and encapsulation efficiency (%) of the electrospun fibres were computed by determining the siponimod content in a known weight of the electrospun product. Briefly, a known mass of the electrospun product (3–6 mg) was dissolved in 10 mL of DMSO and sonicated (Elmasonic S10, Elma Schmidbauer, GmbH, Germany) for 20 min to ensure complete drug release before dilution in the mobile phase and quantification of siponimod by HPLC as described in section 2.5. The practical drug content (% w/w) and encapsulation efficiency (%) were calculated using the following equations:

$$\text{Practical drug content}(\%) = \frac{\text{mass of the drug in implant}}{\text{implant weight}} \times 100\% \quad (1)$$

$$\text{Encapsulation efficiency}(\%) = \frac{\text{Practical drug content (w/w)}}{\text{Theoretical drug content (w/w)}} \times 100\%. \quad (2)$$

2.7. Siponimod release from the electrospun fibres *in vitro*

2.7.1. Siponimod release in phosphate-buffered saline (PBS). The potential of the implant to sustain siponimod release *in vitro* was evaluated using previously described protocols for evaluating drug release from ocular implants.[34] Si : PLGA (4 : 100) and Si : PLGA (8 : 100) were selected as the final formulations to test the drug release based on pilot results that showed that the steady-state siponimod concentration from both implants was above its $IC_{50}$for $S1PR_1$. Given the high cost and limited availability of siponimod, we focused on evaluating implants with lower drug loads. Before the release experiments, the exact mass of Si : PLGA (4 : 100) and Si : PLGA (8 : 100) implants were recorded, and implants were added to a glass vial containing 3 mL of PBS (pH 7.4 ± 0.1). The samples were incubated at 37 °C in a linear shaking water bath (GLS Aqua 18 plus; Grant Instrument, Cambridgeshire, UK). At predetermined intervals, the entire release medium (3 mL) was collected and immediately replaced with 3 mL of fresh PBS. Sampling intervals were determined based on the investigation of siponimod stability in solution (unpublished data). Before HPLC analysis, the collected samples were filtered through a 0.22 μm cellulose acetate filter. Each sample was analysed twice, and the experiment was independently repeated six times (n = 6). The similarity between the release profiles of different formulations was calculated using the similarity factor described in section 2.12.

2.7.2. Siponimod release in porcine vitreous. Siponimod release from the electrospun implants and the stability of the remaining implant in porcine vitreous were investigated *in vitro*. Eyes were obtained from pigs under other ethically and regulatory-approved studies at UCC and frozen before vitreous extraction. They were kept on ice during the extraction process, which involved incising the eyes open with a surgical blade and gently separating the frozen vitreous from the surrounding tissue. The isolated vitreous was thawed on ice before being centrifuged at 4500 rpm for 20 min at 4 °C (Rotanta 460r centrifuge, Hettich, Tuttlingen, Germany), followed by filtration using a sterile 0.22 μm filter to eliminate cellular debris and possible bacterial contamination. The resultant filtrate was collected and promptly stored at −80 °C until use.

For release studies, the vitreous was thawed at room temperature before mixing with 1% PENSTREP (penicillin/streptomycin solution; Merck, Ireland). Then, siponimod-loaded implants Si : PLGA (8 : 100) (average weight of 4.261 mg ± 1.586 mg) were each combined with 1 mL of vitreous in Eppendorf tubes and sealed with parafilm. Three separate tubes were designated for each time point (n = 3). The tubes were incubated at 37 °C using a shaker water bath. At predetermined time points (10, 20, 30, 40, 50, 60 and 70 days), the samples were centrifuged at 14 000 rpm for 20 min to separate the release medium (vitreous) and the remaining implant (containing residual siponimod). Siponimod was quantified in both the release medium and the implant.

To quantify siponimod in the release medium, the supernatant was mixed with 1 mL of acetonitrile, vortexed, and then stored at room temperature for 30 min for complete protein precipitation. The samples were then centrifuged at 14 000 rpm for 10 min to remove the sediments. The supernatant was collected, and the sample volume was reduced under vacuum at 25 °C. After drying, the volume of the samples was adjusted using the mobile phase before quantifying siponimod using the established HPLC method described above.

To quantify the remaining siponimod in the implant, the residual implants were collected after centrifugation, washed three times with PBS, and dried under vacuum at 25 °C overnight. Then, the dry implant was weighed, dissolved in 5 mL of DMSO and sonicated for 30 minutes for complete drug extraction. The solution was then diluted in the mobile phase before quantifying siponimod by HPLC, according to the method mentioned above.

2.8. Stability under stress conditions

To assess the physical and chemical stability of the microfibres, the microfibrous implants were stored under stress conditions of 40 °C and 75% relative humidity (RH) in a controlled climate chamber (Memmert, Buchenbach, Germany). At 30, 60 and 90 days, the physical integrity of the stressed samples was monitored using PXRD, and the chemical integrity was observed by the quantitative analysis of the drug content by HPLC.

2.9. Cell culture, Transwell® migration assay and Thiazolyl Blue Tetrazolium Bromide Assay (MTT) assay

Human retinal microvascular endothelial cells (HRMEC) were purchased from Cell Biologics (Chicago, IL) and were grown in the complete growth medium (CGM) as described previously.[15] The Transwell® migration assay was employed to test the ability of the released siponimod to inhibit HRMEC migration. HRMEC (approximately 50 000 cells, passage number 7–9) were suspended in 100 μL of endothelial cell basal medium and were added into the upper chamber of a polyethene terephthalate (PET) Transwell® insert (pore size 8 μm, Sarstedt, Nümbrecht, Germany). The inserts were fitted into a 24-well plate, and the lower chamber was filled with 400 μL of endothelial cell growth medium supplemented with 10% FBS (foetal bovine serum) as a chemoattractant. For experiments containing siponimod, samples from the release experiments in PBS were diluted in the endothelial cell basal medium and added to the Transwell® system to establish a final siponimod concentration of 100 nM in both the upper and lower chambers to avoid any chemical gradient. A control siponimod solution was freshly prepared and diluted in the endothelial cell basal medium. The solution was used to establish a siponimod concentration of 100 nM in the Transwell® system to compare the effect of the released siponimod to the control siponimod. HRMEC were then allowed to migrate towards the high chemoattractant concentration in the lower chamber for 6 h. After the migration period, the inserts were removed and gently washed with PBS, before being fixed in ice-cold methanol for 25 min at 4 °C. Then, the inserts were stained using crystal violet (0.5% w/v), prepared in methanol (20% v/v in water solution) for 30 min. The non-migrating cells from the upper chamber were gently removed using a wet cotton swab. Finally, the inserts were dried at room temperature for

30 min before visualising the migrating cells using light microscopy (BX43 microscope, OLYMPUS®). For each independent experiment (n = 4), at least two transwell inserts were employed per treatment group, three random images were taken per insert, and the migrating cells were counted in four random fields in each image.

The MTT assay was employed to test the effect of the released drug and polymer degradation products on the metabolic activity of HRMEC. Approximately 4 000 cells per well were seeded in a 96-well plate containing CGM and allowed to adhere overnight. On the following day, the culture medium was replaced with fresh CGM containing 100 nM siponimod in PBS from the release experiments at days 30, 63 and 90. After 72 h of incubation, MTT solution was added to each well to achieve a final concentration of 0.5 mg mL^{-1}. The plate was incubated for 2 h, and then, the formazan crystals were dissolved with 100 µl of alkaline DMSO solution (containing 800 mM of ammonia). Absorbance was acquired at 570 nm using a Wallac Victor 2 plate reader (PerkinElmer, USA). For each condition, the average absorbance of three wells (technical replicates) was employed as a single value in the statistical comparison. The experiment was independently conducted four times (n = 4).

2.10. Statistical analysis

The statistical analysis included all the data obtained; no data points were excluded. Descriptive statistics (mean, standard deviation) were used in all figures. The number of independent replicates (n) is shown in the figure legends or table footnote.

The similarity of siponimod release profiles from different electrospun systems was investigated using the similarity factor test using eqn (3) to calculate the F^2 value. The test utilises the number of data points (n), and the percentage of drug released at time t from the reference formulation (R_t) and test formulation (T_t) to calculate the similarity factor (F^2) value. F^2 values equal to or greater than 50 were considered indicative of the similarity of the release profile, suggesting the absence of a significant difference.

$$F^2 = 50\ \log\left\{\left[1 + \frac{1}{n}\sum_{t=1}^{n}(R_t - T_t)^2\right]^{-0.5}\right\} \quad (3)$$

Randomised block ANOVA (full factorial) was used to statistically compare the results of the Transwell® migration assay and the MTT assay, which was performed using IBM® SPSS® version 28. Null hypotheses were rejected for $p < 0.05$, and *post-hoc* (Tukey's multiple comparisons) analysis was conducted.

3. Results

3.1. Production, morphology, and size distribution of the electrospun microfibres

The microfibres were successfully produced using electrospinning of PLGA 85 : 15. This specific grade of PLGA was employed to achieve the maximum extended release properties due to a slower degradation rate arising from the increased hydrophobicity associated with a higher lactic acid content in the copolymer.[35] Electrospinning working conditions were optimised at 8% w/w polymer concentration, 16 kV applied voltage, flow rate of 0.7 mL h^{-1} and 15 cm collecting distance to achieve a continuous, bead-free, microfibrous matte. Polymer concentration (Fig. S1†) and solvent properties (Fig. S2 and Table S2†) were shown to impact the morphology of the electrospun product. The highly volatile DCM produced a bead-free, microfibrous matte of PLGA 85 : 15 at a relatively low concentration of 8% w/w (Fig. S1†) compared to less volatile solvents (*e.g.*, ethyl acetate and DMF), which resulted in beaded or a mix of beads and fibres at the same polymer concentration (Fig. S2†). Electrospun products prepared using PLGA 85 : 15 8% w/w in DCM (Fig. S1†) had a mean fibre diameter of 1.85 ± 0.81 µm (Fig. 1A), and narrow size distribution, with 92.1% of fibres having a diameter between 0.5–3 µm (Fig. 1B). Furthermore, SEM images of the electrospun (ES), drug-free fibres showed nano-sized pores (100–300 nm) along the fibre surface (Fig. 2A and B). Similar porous structures were evident when PLGA was electrospun from DCM at lower concentrations (Fig. S1†) and when PLGA was electrospun from different solvents (Fig. S2†).

Drug-loaded microfibres were produced at different mass ratios; details are outlined in Table 1. Electrospinning of drug-loaded solutions showed a stable jet and continuous microfibre formation. The electrospun fibres showed a high siponimod encapsulation efficiency ranging from 77.68% ± 7.5% to 85.48% ± 8.9% of the loaded drug (Table 1). Incorporation of siponimod at the lowest mass ratio Si : PLGA (0.5 : 100) did not alter the size distribution of the fibres (Fig. 1C and D) or fibre morphology, with individual fibres showing similar nano-pores on the surface similar to drug-free fibres (Fig. 2C). Incorporation of siponimod in higher ratios Si : PLGA (4 : 100), Si : PLGA (8 : 100) and Si : PLGA (12 : 100) resulted in the formation of microfibres with comparable mean fibre diameters of 1.92 ± 1.09 µm, 1.86 ± 0.80 µm, 1.62 ± 0.74 µm, respectively (Table 1), and similar size distributions compared to the drug-free fibres (Fig. 1F, H and J, respectively). However, fibres with higher siponimod concentrations showed distinctively less porous surfaces (Fig. 2D, E and F). This noteworthy reduction in the porosity was also evident from the surface area and pore analysis (method described in the ESI section S1.3 and results are presented in Table S3).† The surface area of drug-free ES PLGA (Fig. 2A and B) showed a total BET surface area of 5.8 $m^2\ g^{-1}$, with a pore volume of 0.042 $cm^3\ g^{-1}$ (Table S3, ESI data†). Notably, Si : PLGA (12 : 100) (Fig. 2F) showed a noticeably smaller surface area of 3.9 $m^2\ g^{-1}$ and a reduced pore volume of 0.007 $cm^3\ g^{-1}$ (Table S3†). Finally, the contact angle measurement of the electrospun mattes showed an increase from 106.52° ± 3.97° for ES PLGA to 114.00° ± 19.98° for Si : PLGA (12 : 100) (Table S4†); however, this increase was not statistically significant ($p > 0.05$).

3.2. Physiochemical properties of the electrospun microfibres

The thermal behaviour of unprocessed siponimod, unprocessed PLGA and their electrospun formulations was investi-

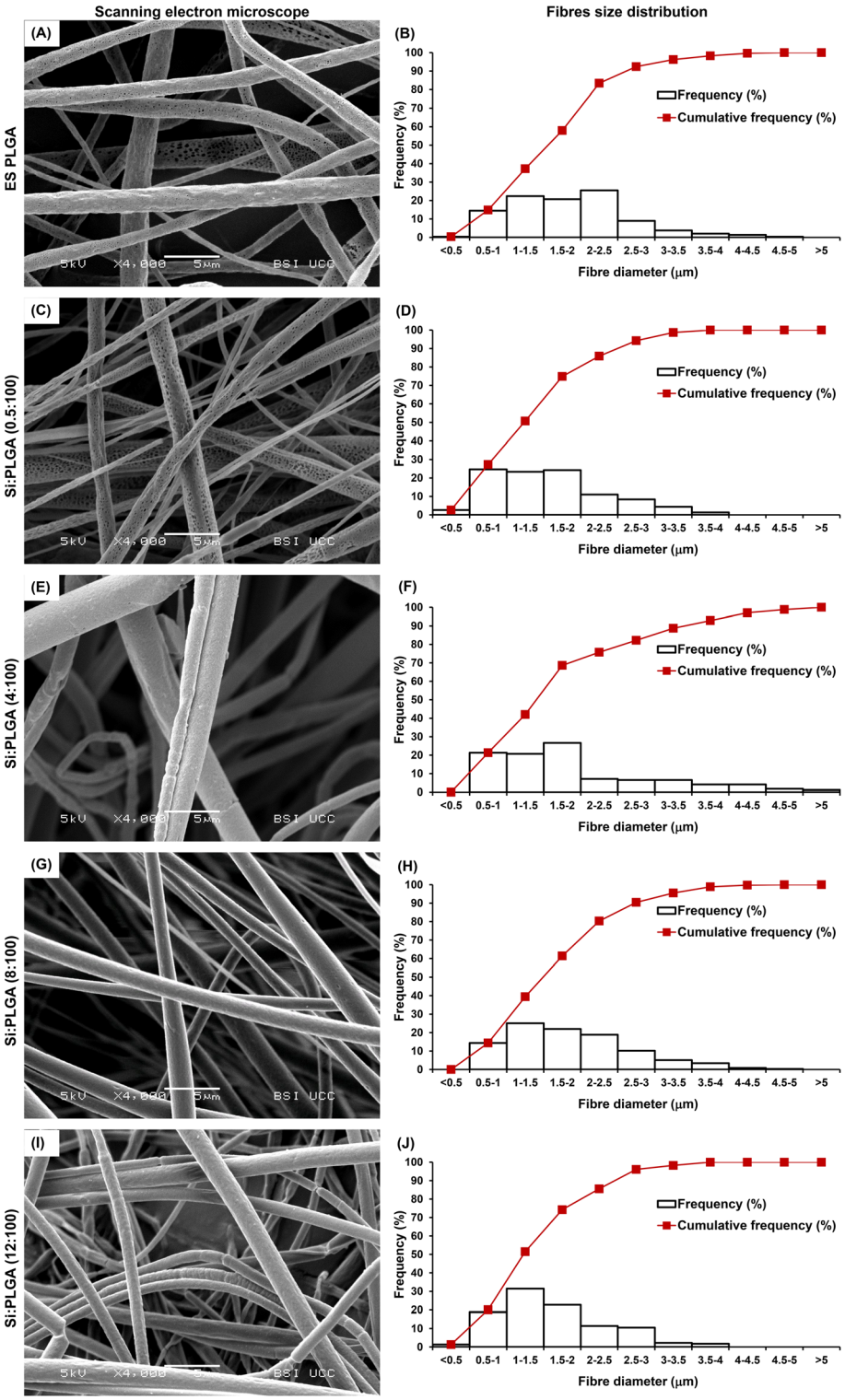

Fig. 1 Representative scanning electron micrographs (left column) and size distribution histograms (right column) of electrospun PLGA 85 : 15 (ES PLGA; panels A and B), Si : PLGA (0.5 : 100) in panels C and D, Si : PLGA (4 : 100) in panels E and F, Si : PLGA (8 : 100) in panels G and H and Si : PLGA (12 : 100) in panels I and J. Details of each electrospun system are presented in Table 1. All scanning electron micrographs were captured at the same magnification (×4000) and the scale bar shown on each image is 5 μm.

gated using DSC, Fig. 3A. Unprocessed siponimod showed a melting endotherm characteristic of crystalline materials with T_m of 115.5 °C (Fig. 3A and Table 2). The thermogram of unprocessed PLGA 85 : 15 shows a characteristic glass transition (T_g) at 54.9 °C followed by structural relaxation,[36] with an extrapolated decomposition temperature of 336.5 °C

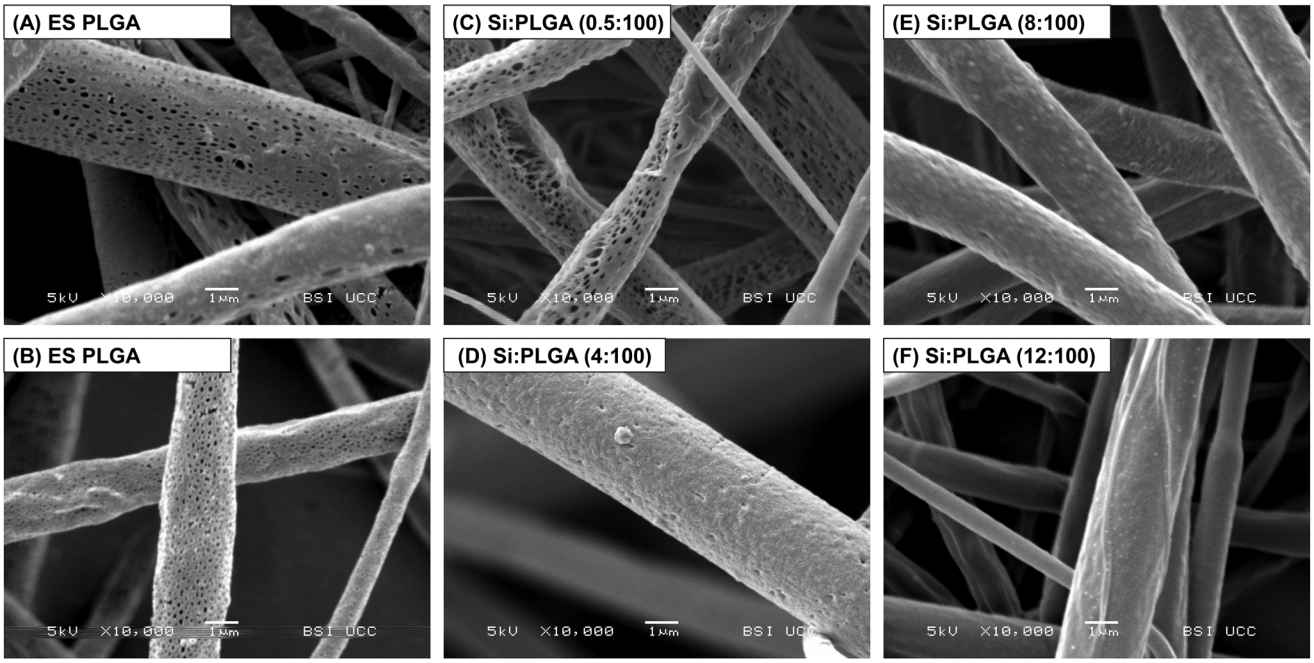

Fig. 2 Representative scanning electron micrographs showing the surface morphology of the electrospun fibres. (A and B) Drug-free electrospun PLGA 85 : 15 (ES PLGA), (C) shows Si : PLGA (0.5 : 100), (D) shows Si : PLGA (4 : 100), (E) shows Si : PLGA (8 : 100), and (F) shows Si : PLGA (12 : 100). Details of each electrospun system are presented in Table 1. All SEM images were taken at the same magnification (×10 000) and the scale bar (1 μm) is shown on each image.

(Table 2 and Fig. S4†). This correlates well with the published data on the same polymer.[37] Electrospinning did not change the thermal behaviour of PLGA. The electrospun PLGA 85 : 15 fibres (ES PLGA) show a comparable T_g of 55.2 °C and extrapolated decomposition temperature of 333.14 °C (Table 2 and Fig. S4†). Electrospun PLGA fibres containing siponimod in different mass ratios exhibited polymer T_g at lower temperatures than unprocessed and electrospun PLGA (Fig. 3A and Table 2). The maximum reduction in T_g was ~5 °C, and occurred with the highest siponimod ratio (Si : PLGA (12 : 100)), Fig. 3A. Furthermore, drug-loaded fibres showed a reduction in the decomposition temperature (extrapolated decomposition onset temperature and the 1st derivative peak temperature) compared to drug-free fibres (Table 2). The magnitude of reduction was proportional to the siponimod ratio in the fibre, up to Si : PLGA (8 : 100). Additionally, no crystalline melting endotherm corresponding to siponimod melting was detected in the drug-loaded electrospun microfibres, even at the highest ratio of siponimod. This suggests that siponimod is molecularly dispersed in an amorphous state within the polymer matrix (Fig. 3A). The glass transition of amorphous siponimod was determined from the heat–cool–heat thermal analysis of the unprocessed drug. The 2nd heating thermogram showed the loss of the crystalline melting endotherm and the presence of a T_g at 44.7 °C.

PXRD was performed to determine the physical form of PLGA and siponimod in their unprocessed and electrospun forms and confirm the hypothesised amorphisation of siponimod in the electrospun fibres. The diffractograms of siponimod, PLGA and the prepared fibres are presented in Fig. 3B. No significant peaks were recorded at 2θ values greater than 60°. Consequently, only data between 3–60° are shown. The XRD pattern of the unprocessed siponimod powder shows a diffraction pattern characteristic of crystalline material with distinctive sharp peaks recorded at the 2θ values of 7.7°, 10°, 11.5°, 12.1°, 14.31°, 15.52°, 17.3°, 18°, 19.24°, 20.91°, 21.88° and 23.26° (Fig. 3B). The X-ray diffraction pattern of unprocessed PLGA shows a broad hump with no distinctive peaks, which is characteristic of amorphous materials (Fig. 3B). Similar observations were made in the case of the drug-loaded microfibres (Fig. 3B).

3.3. Interaction between siponimod and PLGA

FTIR was employed to investigate the molecular changes and possible interactions between PLGA and siponimod (chemical structure in Fig. 4B). The FTIR spectra of unprocessed siponimod, unprocessed PLGA, drug-free fibres, and siponimod-loaded fibres are shown in Fig. 4. The FTIR spectrum of unprocessed PLGA 85 : 15 shows characteristic absorbance bands at 2945 cm^{-1} and 2993 cm^{-1} that can be attributed to the aliphatic C–H stretch (Fig. 4A). The strong absorbance band at 1750 cm^{-1} can be attributed to the carbonyl (C═O) stretch, while the absorbance bands at 1184 cm^{-1} and 1086 cm^{-1} can be attributed to the ester C–O stretches (Fig. 4A). The FTIR spectrum of PLGA agrees with previously published spectra of the polymer.[37,38] Unprocessed siponimod shows an FTIR spectrum that correlates to its functional groups, with a weak absorption band of (O–H) stretch between 2985–2856 cm^{-1}

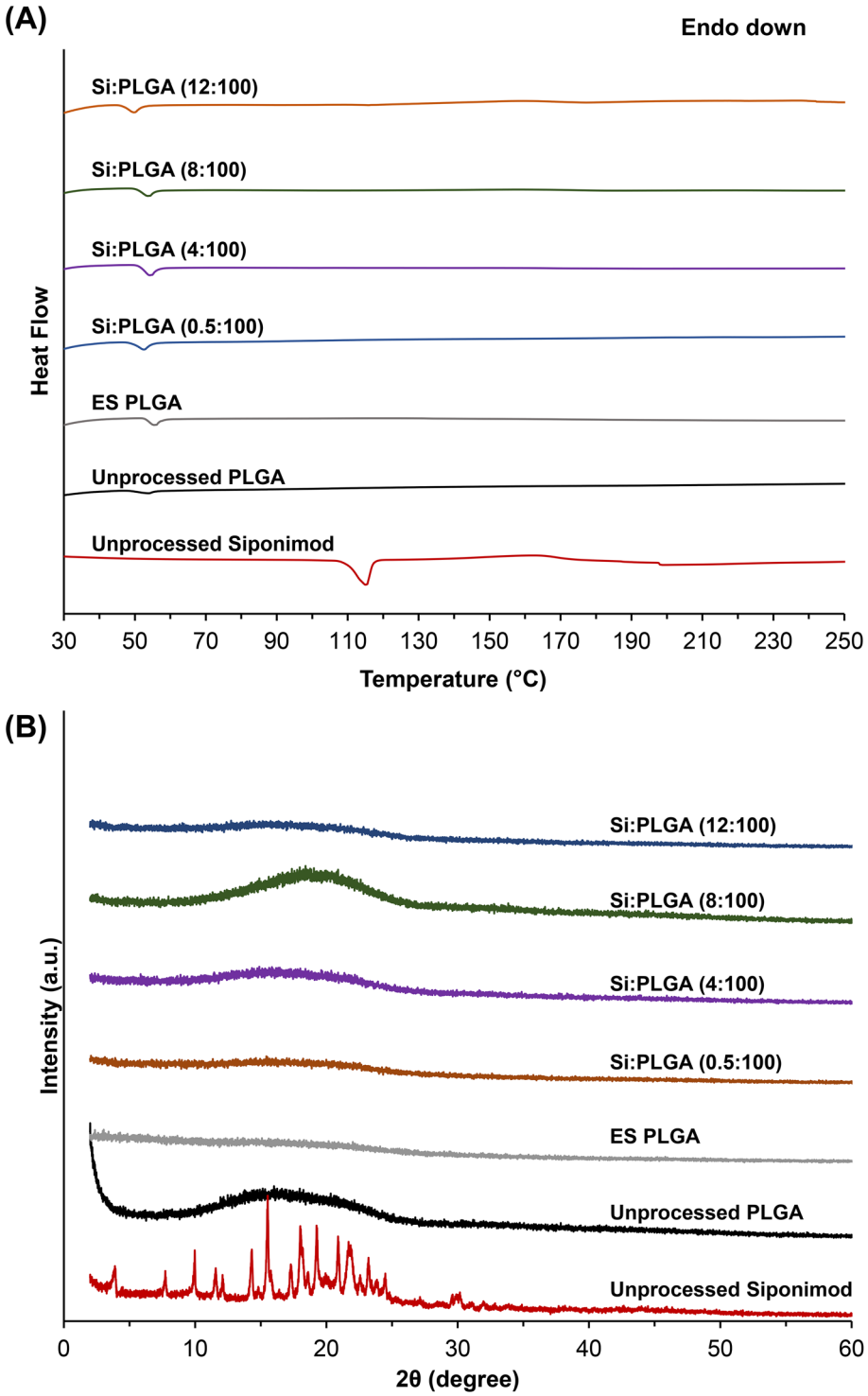

Fig. 3 Physical characterisation of the unprocessed components and the electrospun fibres. Representative (A) DSC thermograms and (B) X-ray diffractograms of unprocessed siponimod, unprocessed PLGA 85 : 15, ES PLGA and different siponimod-loaded electrospun fibres. Details of each electrospun system are presented in Table 1.

and absorbance bands of aliphatic and aromatic C–H stretches between 2845–2830 and 3045–2948 cm^{-1}, respectively. The absorption band of carbonyl group stretch (C═O) can be found at 1589 cm^{-1}, which fuses with the weak absorption band of conjugated C═N stretch in the oxime, appearing as a small shoulder at 1561 cm^{-1}. The O–H bending can be allocated to the medium absorption band detected at 1441 cm^{-1}. Additionally, the absorption bands at 1118 cm^{-1} and 944 cm^{-1}

Table 2 The glass transition temperature (T_g), melting peak (T_m) and decomposition onset (°C) of unprocessed and amorphous siponimod, PLGA and different electrospun formulations

Drug-loaded composition	Glass transition temperature (T_g) (°C)	Melting endotherm (T_m) (°C)	Extrapolated decomposition onset temperature[a] (°C)	1st derivative peak temperature (T_p)[b] (°C)
Unprocessed siponimod (crystalline)	nd[c]	115.5	nd	nd
Amorphous siponimod	44.7	nd	nd	nd
Unprocessed PLGA 85 : 15	54.9	nd	336.5	368.6
ES PLGA	55.2	nd	333.1	366.3
Si : PLGA (0.5 : 100)	53.2	nd	330.7	362.09
Si : PLGA (4 : 100)	54.4	nd	318.6	347.5
Si : PLGA (8 : 100)	54.0	nd	310.74	351.51
Si : PLGA (12 : 100)	49.5	nd	310.73	334.07

[a] Decomposition extrapolated onset temperature is calculated from the TGA thermograms (ESI methods and Fig. S4†). [b] 1st derivative peak temperature (T_p) represents the temperature of maximum decomposition rate and is calculated from the 1st derivative of the TGA thermograms. [c] not detected or determined (nd).

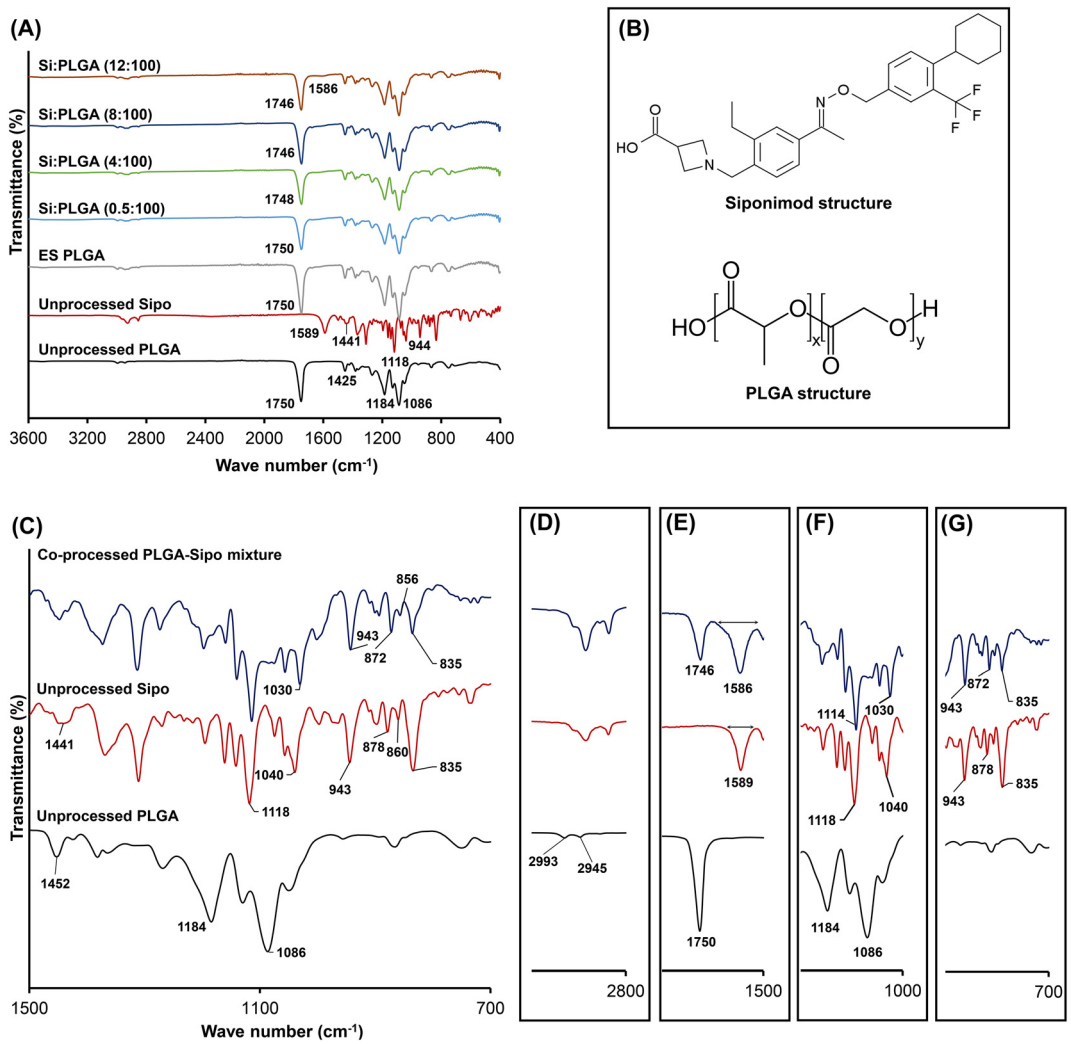

Fig. 4 Representative FTIR spectra investigating siponimod and PLGA 85 : 15 interactions and their chemical structures. (A) FTIR spectra of unprocessed PLGA 85 : 15, unprocessed siponimod, electrospun PLGA (ES PLGA) and siponimod-loaded electrospun fibres at different loadings. Details of the electrospun fibres are presented in Table 1. (B) The chemical structures of siponimod and PLGA. (C) FTIR spectra of unprocessed PLGA, unprocessed siponimod and their co-precipitated mixture from DCM in a 1 : 1 weight ratio. (D–G) Highlighted excerpts showing the recorded changes in specific peaks in the co-processed sample. (D) Shows broadening and an increase in the intensity of the stretching vibration corresponding to the O–H stretch (originating from siponimod) in the co-processed sample, (E) shows the broadening (double head arrow) of the carbonyl group stretch (originating from siponimod) in the co-processed sample and shifting to a lower wavenumber, (F) shows substantial reduction in intensity and alterations in the shape and position of the absorption bands corresponding to C–O stretching in the co-processed sample (originating from PLGA and detected initially at 1184 cm^{-1} and 1086 cm^{-1}), and (G) showing important changes in the intensity, shape or location of the peaks originating from siponimod at 835 cm^{-1} and 878 cm^{-1} (Fig. 4G).

can be attributed to the ester C–O stretch and the oxime ether N–O stretch, respectively (Fig. 4A and C). Peak assignments are consistent with the previously published data for the same functional groups.[39,40]

The FTIR spectrum of electrospun PLGA (ES PLGA) was comparable to that of the unprocessed PLGA. The siponimod-loaded PLGA fibres Si : PLGA (0.5 : 100), Si : PLGA (4 : 100) and Si : PLGA (8 : 100) showed comparable spectra to that of the electrospun and unprocessed PLGA with minor changes including shifting and broadening of PLGA's C═O stretch at 1750 cm^{-1}. Siponimod absorbance bands were not detected in the spectra of these fibres due to the low % of the drug in the samples (Fig. 4A). FTIR spectrum of Si : PLGA (12 : 100) showed the characteristic bands of PLGA with the C═O stretch shifted to a lower wavenumber. Furthermore, a weak signal of the C═O stretch originating from siponimod at 1589 cm^{-1} can be observed as a broad band at a lower energy (1586 cm^{-1}).

To further investigate siponimod and PLGA interaction, the FTIR spectrum of a co-precipitated sample with equal weight ratios of siponimod and PLGA 85 : 15 was also recorded (Fig. 4C). The spectrum shows noticeable broadening and an increase in the intensity of the O–H stretching vibration originating from siponimod (originally detected between 2985–2856 cm^{-1}, Fig. 4D). Significant broadening of the (C═O) stretching band originating from siponimod is also evident (Fig. 4E). Furthermore, substantial changes in the fingerprint region (between 1200 cm^{-1} to 700 cm^{-1}) were noticed. These include a reduction in intensity and alterations in the shape and position of the absorption bands corresponding to C–O stretches in PLGA (detected initially at 1184 cm^{-1} and 1086 cm^{-1}) (Fig. 4F), changes in the shape and a shift to a lower wavenumber (1030 cm^{-1}) of the absorption band originating from siponimod at 1040 cm^{-1}. Changes in the intensity, shape, or location of the peaks originating from siponimod at 835 cm^{-1} and 878 cm^{-1} (Fig. 4G) are also evident.

3.4. Siponimod distribution in the electrospun microfibres

Siponimod presence and distribution within the electrospun fibres were investigated using Raman spectroscopy. Only fibres with high ratios of siponimod (Si : PLGA (8 : 100) and Si : PLGA (12 : 100)) were analysed to improve the signal sensitivity. Raman spectra of unprocessed components and electrospun structures are presented in Fig. 5. PLGA is a Raman-active polymer and tends to produce a significant background signal. Therefore, two regions were selected where the vibrational peaks of siponimod have sufficient Signal Background Ratio (SBR) compared to PLGA. In the fingerprint region, siponimod shows a characteristic strong duplet at 1601.8 and 1614.6 cm^{-1} and a single peak of weak intensity at 1563.6 cm^{-1} (Fig. 5A). In the high-energy region, a distinct peak at 2855.3 cm^{-1} originates from siponimod and does not interfere with the PLGA signal (Fig. 5B). The Raman signal from siponimod in the PLGA matrix was used to build a high-resolution microscopic Raman image to understand the drug distribution among the individual electrospun fibres. Fig. 5C and D show an *X*–*Y* map of the surface of the microfibre. The confocal system is

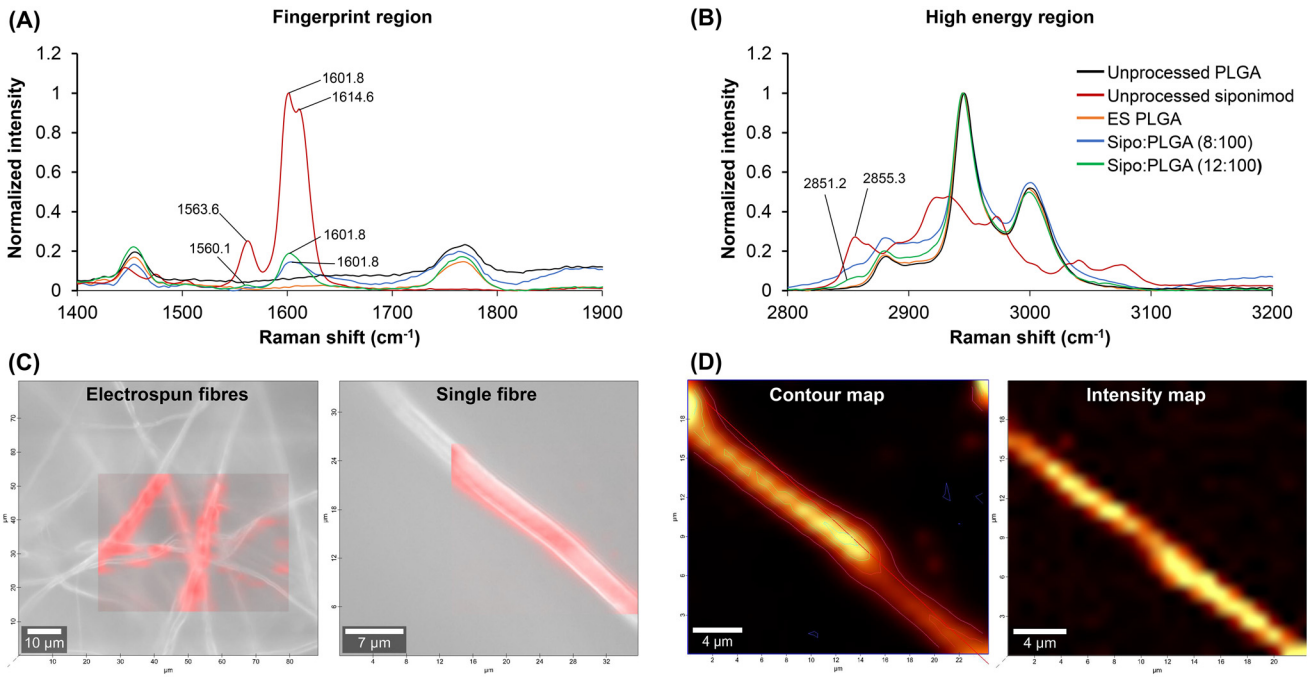

Fig. 5 Raman spectra of unprocessed PLGA, unprocessed siponimod, ES PLGA, Si : PLGA (8 : 100), and Si : PLGA (12 : 100) from (A) 1400–1900 cm^{-1} and (B) 2800–3200 cm^{-1}. (C) Raman images of the siponimod signal overlayed on confocal images in electrospun fibres (left) and a single fibre (right). The red colour shows the Raman intensity collected from the drug. (D) Contour map (left) and intensity map (right) are shown to better view the intensity of drug distribution in the *X*–*Y* plane.

focused on the surface of an individual fibre, and spectra were collected at individual points with an acquisition time of 25 seconds. Precisely, 400 points were measured in the *X*–*Y* plane with 20 points per line in the *X* direction and 20 lines per image in the *Y* direction for a 30 μm length of the fibre (Fig. 5C). The contour lines depict the Raman intensity variation in a single *X*–*Y* plane (Fig. 5D). This was followed by 3D scans of the same fibre. This was achieved by stacking Raman signals from similar *X*–*Y* planes in the *Z* direction. To check the *Z* (depth) distribution along the fibre, *Z* scans were performed 10 μm into the depth of the sample. The 3D scans and *Z* maps are shown in Fig. S5 and S6,† respectively. The maps show that the siponimod signal originates from homogenously distributed points along the examined area, which suggests homogenous and intact drug distribution within the fibre matrix. Similar maps were performed for five different locations in the sample to ensure uniformity. Larger area maps (200 × 160 μm) with lower resolution were also performed at different locations on the surface, and similar Raman signals from the drug were observed.

3.5. Siponimod release from the electrospun implant and kinetic modelling of the release profile

Siponimod release from the electrospun Si : PLGA (4 : 100) and Si : PLGA (8 : 100) implants was investigated in PBS (20 mM, pH = 7.2 ± 0.2). Drug release from the Si : PLGA (8 : 100) implant formulation was also investigated in porcine vitreous. These implants were selected as the final formulations to test the release behaviour because pilot studies showed that the steady-state siponimod concentration was above its IC_{50}. Given the high cost and limited availability of siponimod, we focused on evaluating implants with lower drug loads. However, it is reasonable to expect that the implant with a higher drug load Si : PLGA (12 : 100) will have comparable release kinetics. Additionally, it is important to highlight that implants with lower loading doses of siponimod might reduce systemic drug concentration and associated side effects, as higher doses of siponimod were associated with a higher risk of negative chronotropic effects[41]

Fig. 6A and B show the cumulative siponimod release from Si : PLGA (4 : 100) and Si : PLGA (8 : 100) in PBS and the remaining amount of siponimod in the implants after the release period, respectively. Both drug-loaded implants showed comparable release behaviour in PBS (Fig. 6A), with an initial burst release of approximately 5% in the first 5 days. This was followed by a sustained steady release of approximately 30% of the loaded drug over 90 days (Fig. 6A). The similarity of siponimod release pattern from both formulations is also reflected in the similarity factor test (F^2 value of 81). However, it is important to note that in both experiments, the cumulative drug release at the latest time point was below 85%, which could impact the results of the F2 test. The data obtained from drug release experiments were fitted to different kinetic models using the equations described in the ESI methods (section S1.4†),[42,43] and the results are summarised in Table 3. The fitting data shows that the Higuchi release model provided an excellent fit to the experimental data (R^2 of 0.996 and 0.999 for Si : PLGA (4 : 100) and Si : PLGA (8 : 100), respectively). After 90 days, siponimod cumulative % release was 30.6% from Si : PLGA (4 : 100) and 33.2% from Si : PLGA (8 : 100), while 58.7% and 55.0% of the loaded drug remained unchanged in Si : PLGA(4 : 100) and Si : PLGA (8 : 100) implants, respectively.

The concentration of the released siponimod in the release medium (μg mL^{-1}) at each time point is presented in Fig. 6C. These data show that the Si : PLGA (4 : 100) and Si : PLGA (8 : 100) implants maintained siponimod concentration at approximately 1 μg mL^{-1} and 1.8 μg mL^{-1}, respectively (Fig. 6D). The cumulative release of siponimod from Si : PLGA (8 : 100) in porcine vitreous was comparable to the release in PBS, with a similar pattern of initial burst release (6.8% after 10 days) followed by steady, sustained release over 70 days. After 70 days, approximately 30% of the loaded siponimod was released into the vitreous, with 60.8% of the drug remaining in the implant.

After 30 and 70 days in the release media (PBS or porcine vitreous), the structures of the fibre in the drug-free (ES PLGA) and the drug-loaded (Si : PLGA (8 : 100)) implants were examined using SEM (Fig. 6E and F). After 30 days of incubation in PBS, both ES PLGA and Si : PLGA (8 : 100) fibres largely retained their morphology showing uniform structure. An increase in the surface roughness and fibre porosity was noticed in both electrospun systems. Similar changes were observed after the implants were incubated in porcine vitreous. After incubation in PBS for 70 days, ES PLGA showed a significant loss of fibre structure, increased porosity and formation of fused irregular polymer mass. A similar pattern was observed when ES PLGA was incubated in the porcine vitreous. However, while incubation of Si : PLGA (8 : 100) in PBS for 70 days led to thinning and pore formation, the fibres retained their cylindrical shape and intact structure. Similar changes were noticed when Si : PLGA (8 : 100) was incubated in porcine vitreous for the same period.

3.6. Effect of siponimod on human retinal microvascular endothelial cell (HRMEC) migration and metabolic activity

Siponimod released from Si : PLGA (4 : 100) and Si : PLGA (8 : 100) at day 90 was used to test the ability of the released drug to inhibit HRMEC migration towards the chemoattractant, 10% FBS (Fig. 7A and B). Standard siponimod solution (100 nM) significantly inhibited HRMEC migration towards 10% FBS with the number of migrating cells decreased to 22.8 ± 9.3% of cell migration towards FBS control (Fig. 7A). This concentration was employed based on our previous studies, which showed that siponimod (100 nM) is an effective concentration *in vitro* for reducing endothelial cell migration without adversely affecting the metabolic activity of the cells or cellular proliferation.[15]

Siponimod (100 nM) released from Si : PLGA (4 : 100) and Si : PLGA (8 : 100) implants inhibited HRMEC migration towards 10% FBS. Similar to the standard drug solution control, the number of migrating cells reduced to 26.9 ± 8.7% and 21.3 ± 4.3% of the FBS control (73.1% and 78.7%

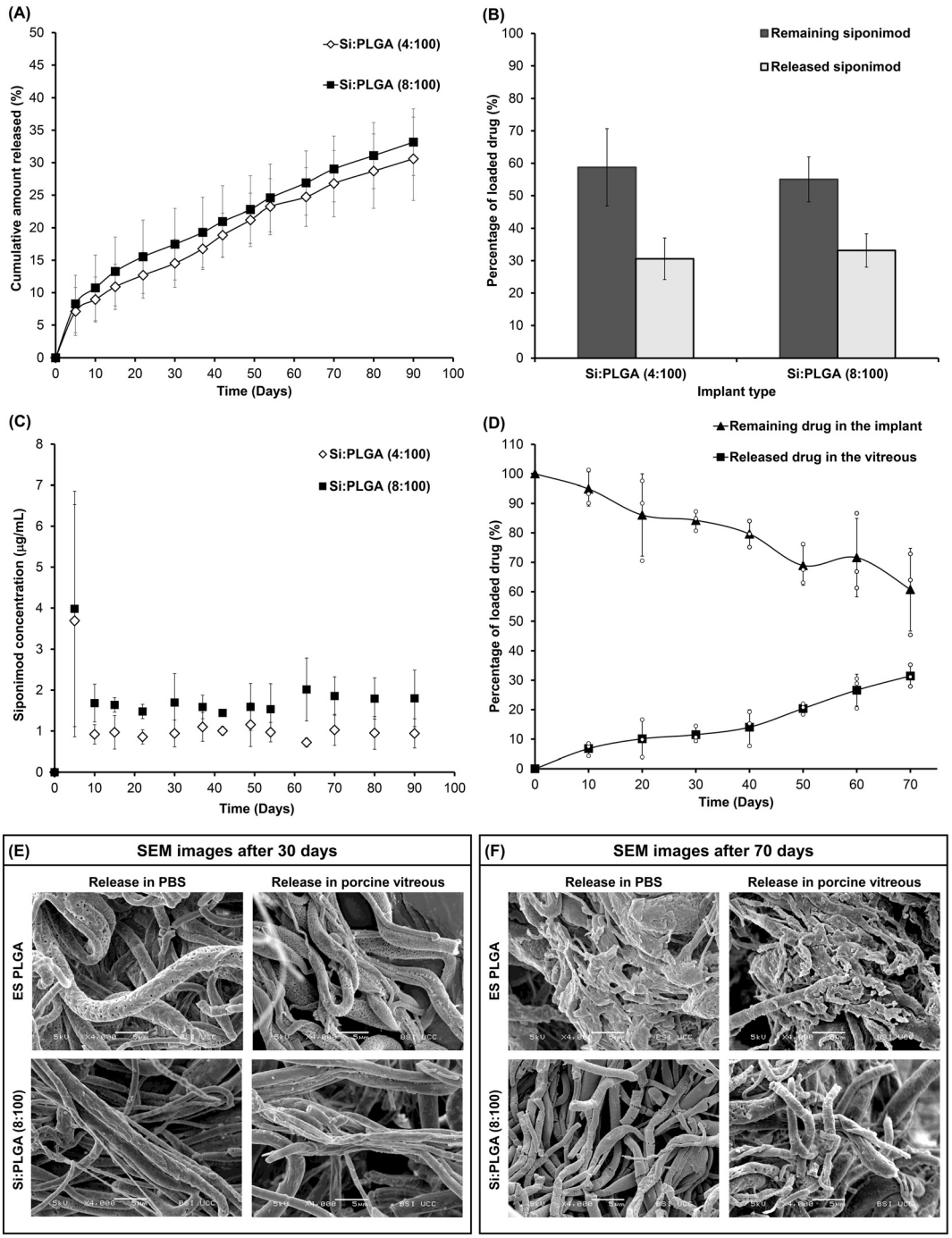

Fig. 6 *In vitro* siponimod release from the electrospun implants in phosphate-buffered saline (PBS) and porcine vitreous. (A) % cumulative siponimod release from Si : PLGA (4 : 100) and Si : PLGA (8 : 100) over 90 days in PBS (n = 6). (B) Comparison of the % drug released and remaining in both Si : PLGA (4 : 100) and Si : PLGA (8 : 100) implants after 90 days in PBS. (C) Siponimod concentration (μg mL^{-1}) in PBS at different time points over 90 days (n = 3). (D) Siponimod release from Si : PLGA (8 : 100) in porcine vitreous, with the curve showing the % drug released (black squares) and the % drug remaining (black triangles) at each time point over 70 days (n = 3). (E) and (F) Representative scanning electron micrographs of the drug-free (ES PLGA) and Si : PLGA (8 : 100) implants after drug release in PBS or porcine vitreous over 30 and 70 days, respectively (voltage: 5 kV, scale bar 5 μm).

reduction in cell migration) for Si : PLGA (4 : 100) and Si : PLGA (8 : 100), respectively. No statistically significant difference was found between the standard siponimod solution and the effect of siponimod in Si : PLGA (4 : 100) and Si : PLGA (8 : 100) release media (Fig. 7A). This suggests that the PLGA degradation products in the medium had no effect on HRMEC migration or siponimod pharmacological activity.

Table 3 The release kinetics model parameters describing cumulative siponimod release from drug-loaded electrospun fibres showing the model constant (K) and the correlation coefficient (R^2) for each model

	Drug release in PBS			
	Si : PLGA (4 : 100)		Si : PLGA (8 : 100)	
Model	K	R^2	K	R^2
Zero-order	0.323	0.963	0.335	0.942
First order	0.018	0.947	0.015	0.921
Higuchi model	3.031	0.996	3.354	0.999

The effect of the released drug and accompanying PLGA degradation products on HRMEC metabolic activity was investigated. Incubation of HRMEC with the release medium from Si : PLGA (4 : 100) (Fig. 7C) and Si : PLGA (8 : 100) (Fig. 7D) has no statistically significant effect on the metabolic activity of HRMEC at any of the tested time points. This suggests that neither siponimod nor PLGA degradation products produce any toxic effects on HRMEC.

3.7. Stability under stress conditions

To investigate the physical stability of the microfibrous implants and the loaded drug's chemical stability under stress conditions, the systems were incubated at 40 °C and 75% relative humidity for 3 months. The PXRD diffractograms taken on days 30, 60 and 90 show that the drug-free and drug-loaded electrospun fibres were able to retain their physical state for 90 days. No crystalline peaks that can be attributed to siponimod or PLGA recrystallisation were noticed (Fig. 8A). Furthermore, analysis of siponimod showed that no significant drug loss was evident with approximately 82.4 ± 15.4 and 87.6 ± 7.1% of the loaded drug being detected after 90 days of incubation.

4. Discussion

Ocular neovascular diseases are debilitating, sight-threatening disorders that are currently treated by lifelong monthly injections of biological angiogenesis inhibitors. Such treatment protocols are associated with unsatisfactory gains in visual

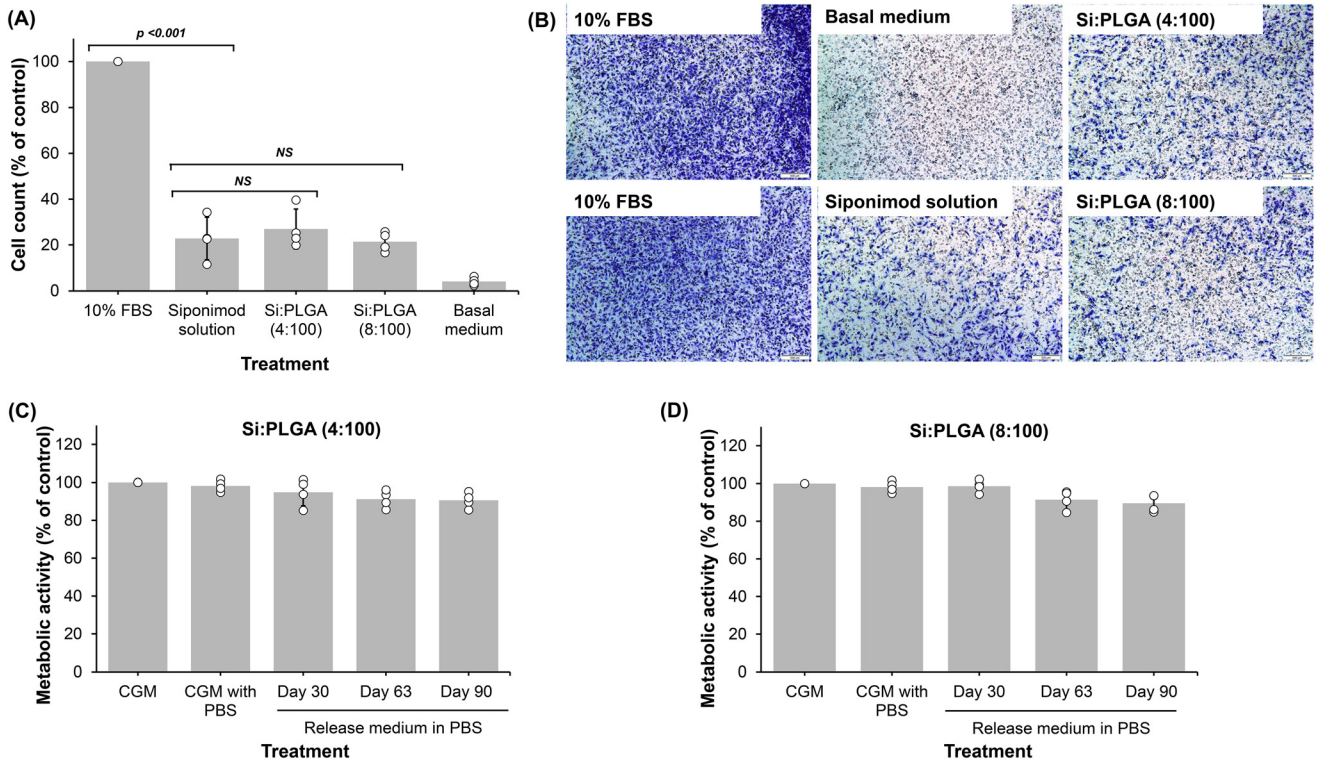

Fig. 7 The effect of the released siponimod on (A and B) human retinal microvascular endothelial cell (HRMEC) migration towards 10% foetal bovine serum (FBS) and (C and D) metabolic activity. (A) Migrating cell count (% of control) on the bottom side of the membrane in the presence of 100 nM of freshly prepared siponimod solution (siponimod solution), or 100 nM of siponimod collected at day 90 from Si : PLGA (4 : 100) or Si : PLGA (8 : 100). Basal medium represents cell migration towards basal endothelial medium (0% FBS; negative control). The bars show the average, the error bars show the standard deviation, and the white circles show the independent experiments in each treatment group (n = 4). (B) Representative images from the bottom side of the Transwell® chamber after the migration period of 6 h showing different cell migration patterns. (C) and (D) Metabolic activity of HRMEC, measured using the MTT assay, following 72 h treatment with the release medium. The medium, containing 100 nM of siponimod was collected from release experiments in PBS for (C) Si : PLGA (4 : 100) and (D) Si : PLGA (8 : 100) on days 30, 63, and 90. The bars show the average, the error bars show the standard deviation, and the white circles show the independent experiments in each treatment group (n = 4). No statistically significant difference was found between the metabolic activity of cells treated with release medium from Si : PLGA (4 : 100) and Si : PLGA (8 : 100) ($p > 0.05$).

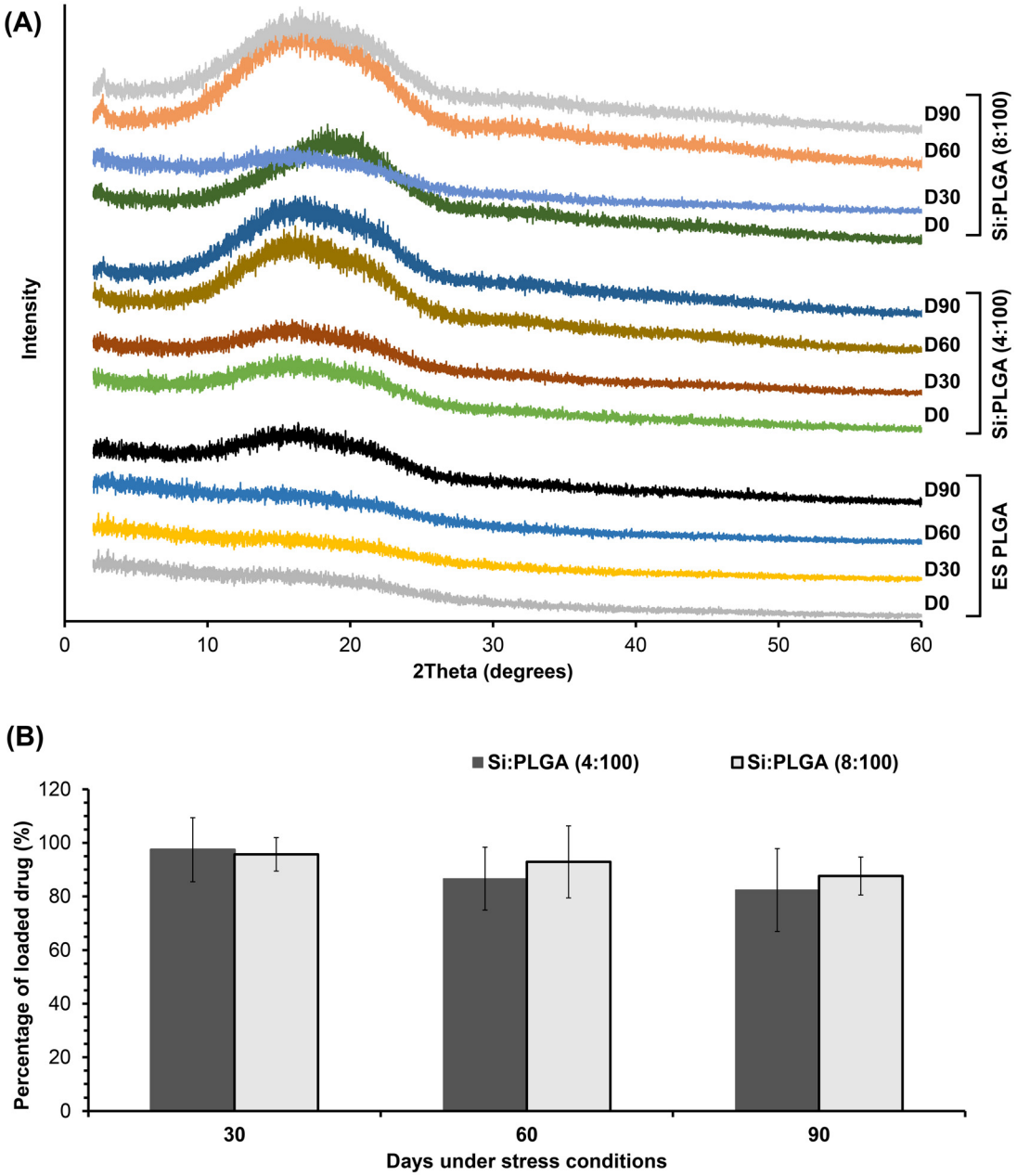

Fig. 8 Stability of the electrospun implants under stress conditions (75% relative humidity and 40 °C) for 3 months. (A) PXRD of the drug-free electrospun PLGA (ES PLGA), Si : PLGA (4 : 100) and Si : PLGA (8 : 100) at days 0, 30, 60 and 90. (B) The remaining percentage of loaded siponimod (average drug content at time zero was set to 100%) in Si : PLGA (4 : 100) and Si : PLGA (8 : 100) after 30, 60 and 90 days of storage under stress conditions. No statistically significant difference was found between the drug content at the tested time points for Si : PLGA (4 : 100) and Si : PLGA (8 : 100) ($p > 0.05$) using randomized block ANOVA.

acuity, poor patient adherence and multiple side effects related to frequent intravitreal injections. Siponimod is an FDA-approved drug for multiple sclerosis with a novel inhibitory effect on ocular angiogenesis that has shown effectiveness *in vitro* and *in vivo*.[15] Herein, we successfully fabricated a microfibrous implant requiring less frequent administration than current therapies for sustained intravitreal delivery of siponimod. Siponimod is a small-molecule angiogenesis inhibitor with a novel mechanism of action and has lower stability and treatment resistance challenges compared to currently approved biologics.

The implant was produced by electrospinning the drug–polymer solution to produce a bead-free, hydrophobic, microfibrous matte. The matte was then cut into squares and rolled into a cylindrical implant, 9 mm in length and 2 mm in diameter (ESI Fig. S3†). These dimensions were chosen considering the diameter of the vitreous cavity of an average human of 17.2 mm (ref. 44) and considering the dimensions of the cur-

rently approved implants for intravitreal use: OZURDEX® (biodegradable, 6 mm length × 0.46 mm in diameter), ILUVIEN® (non-biodegradable, 3.5 mm length × 0.37 mm in diameter), RETISERT™ (non-biodegradable, 5 mm length × 3 mm width) and SUSVIMO® (8.4 mm length × 3 mm width).[4]

Our data indicate that siponimod was homogenously distributed within the electrospun fibres. Importantly, the drug–polymer interaction reduced the fibres' porosity, which hindered water penetration, slowed the matrix degradation and sustained the drug release for a minimum of 90 days. The released drug after 90 days inhibited retinal microvascular endothelial cell migration, and the remaining drug in the implant after the release period was largely intact. The electrospun systems were stable under accelerated conditions, showing both the physical stability of the amorphous form and the chemical stability of the entrapped drug.

4.1. Siponimod alters the porosity of electrospun fibres due to drug dispersion and drug–polymer interactions

The high volatility of DCM allowed the production of bead-free microfibres (Fig. S2†) at a relatively lower polymer concentration compared to other less volatile solvents under the optimised electrospinning conditions.[45,46] The drug-free fibres showed characteristic nanopores (~200 nm in diameter) along the fibre structure. Production of porous fibres after electrospinning of hydrophobic polyesters from DCM was previously reported for PLGA[47,48] and poly(lactic acid) (PLA) polymers.[49] Pore formation has been attributed to many factors, including polymer composition, polymer–solvent interaction, solvent vapour pressure and the humidity of the electrospinning environment.[50–52] Interestingly, the incorporation of higher ratios of siponimod resulted in the formation of microfibres with smoother surfaces, an apparent lack of porosity and a noticeable reduction in the BET surface area and pore volume (Table 1, Fig. 2 and Table S3†). The reduced porosity after siponimod incorporation can be explained by the deposition of siponimod as a solid dispersion within the polymer interstitial spaces and the potential interaction between siponimod and PLGA molecules.

The presence of siponimod as a solid dispersion within the PLGA fibres was confirmed using DSC, PXRD and Raman spectroscopy. Thermal analysis of the drug-loaded electrospun systems showed the lack of the crystalline melting endotherm corresponding to siponimod melting (Fig. 3A and Table 2), and the X-ray diffractograms also showed a broad hump characteristic of amorphous materials (Fig. 3B). Both methods confirm that siponimod is available as an amorphous solid dispersion in the PLGA matrix. The Raman maps show that the siponimod signal was homogenously distributed within the fibre structures (Fig. 5, Fig. S5 and S6†), suggesting that siponimod is consistently dispersed within the fibres. Such distribution could alter the morphology of drug-loaded fibres, contributing to the loss of porosity due to siponimod disposition in interstitial spaces.

Furthermore, FTIR analysis confirmed the formation of hydrogen bonds between siponimod and PLGA. The FTIR spectra of Si : PLGA (12 : 100) and the co-precipitated product of siponimod and PLGA 85 : 15 showed distinctive changes indicating hydrogen bond formation (Fig. 4), including significant broadening and shifting to a lower wavenumber in absorption bands associated with hydrogen bond forming groups in both siponimod and PLGA. It is important to highlight that the evident interaction in the co-precipitated siponimod–PLGA mixture does not necessarily simulate the interaction between siponimod and PLGA in the electrospun fibres. However, this experiment strongly suggests the potential interaction between both components when precipitated from DCM, the same solvent used in electrospinning. Similar changes were previously taken as indicators of drug–polymer hydrogen bonding between tetracycline hydrochloride and PLGA,[53] triamcinolone and PEG-PDL[54] and triamcinolone and PLGA.[55] Hydrogen bond formation between siponimod and PLGA explains the ability of siponimod to interfere with the molecular packing and plasticising of the PLGA matrix. This plasticising effect was confirmed by thermal analysis as indicated by the lower T_g temperature and lower decomposition temperature of drug-loaded fibres compared to control fibres (Fig. 3A and Table 2). Similar interactions and outcomes were previously reported for drugs incorporated in electrospun PVA, where hydrogen bond formation between sodium salicylate or diclofenac sodium and PVA were proposed to interfere with polymer molecular packing, resulting in changes in the melting temperature (T_m) of the crystalline polymer.[56] A similar plasticising effect was also reported for prodigiosin and paclitaxel in PLGA-PEG microparticles. In this case, the drug-loaded formulation exhibited lower T_g and a decreased decomposition temperature compared to the control polymer.[57]

The siponimod–PLGA interaction can also contribute to reduced pore formation after electrospinning. For instance, alteration of the morphology of electrospun products owing to drug–polymer interactions was previously reported with tenofovir,[58] where the formation of electrospun fibres with a smooth surface was attributed to hydrogen bonding between the drug and PLGA. In contrast, rough surface fibres occurred when the drug was incorporated into other polymers.

4.2. Siponimod-loaded fibres showed exceptionally extended drug release due to the lack of porosity and presence of hydrogen bonding

Siponimod release from the electrospun Si : PLGA (4 : 100) or Si : PLGA (8 : 100) implants in PBS showed a type II biphasic release, which follows the release of PLGA systems loaded with hydrophobic drugs.[59,60] The biphasic release constitutes an initial burst of less than 10% of the loaded drug and a slow and sustained release of ~30% of the drug load over 90 days (Fig. 6). The release pattern in PBS showed an excellent fit to the Higuchi release model, which describes the drug release from a non-swellable, non-soluble matrix, where the drug concentration in the matrix system exceeds its saturation solubility.[42,61] This suggests that the release of siponimod from the electrospun matrix follows Fickian diffusion, where

the drug release amount is proportional to the square root of time.[62] Additionally, it suggests the rate-controlling step is the diffusion of siponimod through the polymer, not the dissolution of the drug. The initial burst release could be attributed to non-encapsulated drug molecules loosely bound to the fibre surface,[59,60] and the extended and steady drug release can be partially attributed to the significant reduction in the surface area and pore volume of the electrospun fibres. One of the most important factors that governs the drug release rate from polymer matrices is the rate of drug diffusion through the water-filled pores, which is dependent on the extent of porosity and tortuosity of the pore network, drug–polymer interactions, drug hydrophobicity and drug dissolution rate.[63] Therefore, the lack of a porous structure in the siponimod electrospun fibres is a crucial factor contributing to the uniquely long drug release period. A similar association between porosity and higher drug release was previously reported for the release of human growth hormone from PLA and PLGA microspheres,[64] the release of paclitaxel from PLGA disks[65] and the release of salicylic acid from PEG/PLA nanofibres.[66]

It is worth noting that the drug-free electrospun matte (ES PLGA) was significantly hydrophobic (water contact angle of 106.52° ± 3.97°), which is to be expected considering the hydrophobicity of PLGA 85 : 15, the dense microfibrous structure of the matte and the presence of interfibre pores filled with air.[67,68] Incorporating siponimod in the highest ratio Si : PLGA (12 : 100) resulted in a non-significant increase in the contact angle to 114.00°. Contact angle and wettability are less sensitive to small nanopores within the fibres compared to larger interfibre pores (which did not change due to siponimod incorporation).[69] This can explain the non statistically significant increase in the contact angle of Si : PLGA (12 : 100) compared to drug-free fibres. However, the overall porosity still plays a crucial role in drug release as it slows down the rate at which the release medium penetrates the mat, leading to a more controlled and sustained drug release, as previously discussed.

Furthermore, hydrogen bonding between siponimod and PLGA can retard the drug release from the PLGA matrix, contributing to the sustained release profile. This was previously shown for the antiviral drug tenofovir, where hydrogen bond formation between the phosphonic acid group in tenofovir and PLGA was responsible for the slower drug release from the PLGA matrix compared to the faster drug release of the prodrug tenofovir disoproxil fumarate, which lacked the reactive phosphonic acid group.[70] These data suggested that the hydrogen bonding between tenofovir may be necessary for stabilising and inhibiting its release from polyester fibres.

Our results also show that siponimod release from Si : PLGA (8 : 100) in porcine vitreous was comparable to the release profile in PBS. This indicates that the vitreous environment did not have a noticeable effect on siponimod release or the mass loss of the implant, with the implant able to retain siponimod release for a minimum of 70 days.

4.3. Siponimod-loaded fibres showed slower degradation of the PLGA matrix, possibly due to the lack of porosity

The degradative changes observed in drug-free electrospun PLGA fibres after 70 days were comparable to previously reported degradation of electrospun PLGA incubated in aqueous media.[71,72] They showed a significant loss of the fibre structure and the formation of a fused irregular mass. Interestingly, changes in the degradation of siponimod-loaded fibres Si : PLGA (8 : 100) were less substantial, showing slower deformation of the fibre structure and the overall integrity relatively maintained (Fig. 6F). The slower degradation of siponimod-loaded matrices can also be attributed to the lack of porosity, which retards the water diffusion into the fibres slowing the matrix degradation. The change in the degradation behaviour can also be influenced by siponimod's hydrophobicity, which can resist water penetration thereby slowing both matrix degradation and drug release. This effect of drug properties on both the mechanism and rate of polymer degradation was previously shown, where hydrophilic drugs and excipients increased water penetration into the polyester matrix and impacted subsequent hydrolytic changes,[73] while hydrophobic drugs slowed down both processes.[74,75]

4.4. Siponimod amorphous solid dispersion is stable under stress conditions

As previously mentioned, the solid-state characterisation showed that siponimod is homogenously distributed within fibres as an amorphous solid dispersion. This can be concerning as drugs in their amorphous state are typically less stable than their crystalline counterparts and are highly susceptible to recrystallisation over time. However, our results show that under stress conditions (40 °C and 75% relative humidity for 3 months), the electrospun fibres maintained their physical stability, as confirmed by PXRD (Fig. 8), with no evidence of siponimod recrystallisation. Siponimod loaded into the implant showed no significant loss after incubation under stress conditions, as confirmed by the drug content in the fibres over 90 days of incubation (Fig. 8). This physical and chemical stability can be attributed to the presence of a polymer matrix, which can offer significant stabilisation for the dispersed amorphous drug.[76–78] The polymer matrix can reduce the molecular mobility of dispersed drugs, inhibit the molecular recognition required for nucleation and increase the energy required for crystallisation[76–78] resulting in a stable amorphous solid dispersion as previously described.[79,80]

4.5. Released siponimod from implants successfully inhibited retinal endothelial cell migration and did not affect cells' metabolic activity

The concentrations of the released siponimod in the release medium from Si : PLGA (4 : 100) and Si : PLGA (8 : 100) implants were maintained at approximately 1 μg mL^{-1} and 1.8 μg mL^{-1}, respectively (Fig. 6). These concentrations were above the IC_{50} of siponimod at $S1PR_1$ (0.39 nM, 0.000201 μg mL^{-1}) and the highest effective dose that was previously tested

in vitro (100 nM, 0.052 μg mL^{-1}).[15] The released siponimod at day 90 (diluted to 100 nM) inhibits HRMEC migration towards 10% FBS to the same extent as freshly prepared siponimod solution of the same concentration (Fig. 7). Siponimod released from both implants reduced HRMEC migration by more than 70%. This indicates that the drug released after 90 days can produce a pharmacological effect that is comparable to the standard unprocessed drug solution. Furthermore, the release medium from Si : PLGA (4 : 100) and Si : PLGA (8 : 100) had no significant adverse effect on the metabolic activity of HRMEC at days 30, 63 and 90. This indicates the drug loaded in both systems is sufficient to maintain effective angiogenesis inhibition *in vitro* with no toxic effect observed over the experimental timeframe.

5. Conclusion

We fabricated an electrospun microfibrous PLGA implant loaded with siponimod with distinctively reduced porosity for the long-term management of neovascular ocular diseases. The implant sustained siponimod release and maintained its physical and chemical stability for at least three months. Compared to drug-free electrospun fibres, drug-loaded fibres showed a smoother surface and lacked a porous morphology, features that can be partially attributed to drug–polymer interaction. The lack of porosity resulted in a unique prolonged release of siponimod for a minimum of 90 days and significantly slower degradation of the PLGA matrix. The released drug showed comparable efficacy to the freshly prepared standard solution. The siponimod signal was homogenously distributed within the fibre structure as an amorphous solid dispersion. Both physical and chemical stabilities of the drug were maintained over 90 days under stress conditions.

Taking into consideration siponimod's advantages, including its novel mechanism of action and its small molecular weight, in contrast to the currently approved large molecular weight anti-VEGF treatments that require frequent intravitreal injection, the developed implant can also minimise the number of intravitreal injections needed to achieve a satisfactory effect in neovascular ocular diseases. To advance this research, testing the implant's potential side effects and any inflammatory responses *in vivo* is crucial. Thereafter, demonstrating the ocular compatibility and the long-term efficacy of the implant in the relevant disease model are necessary.

Author contributions

Rasha A. Alshaikh: conceptualization, data curation, formal analysis, methodology, validation, investigation, visualization, writing – original draft. Krishnakumar Chullipalliyalil: data curation, formal analysis, methodology, investigation, resources, visualization, software, writing – original draft. Christian Waeber: conceptualization, funding acquisition, investigation, methodology, project administration, resources, writing – review & editing, supervision. Katie B. Ryan: conceptualization, funding acquisition, investigation, methodology, project administration, resources, writing – review & editing, supervision.

Data availability

The data supporting this article have been included as part of the ESI.†

Conflicts of interest

There are no conflicts to declare.

Acknowledgements

This work was supported by the Irish Research Council for Science, Engineering and Technology (IRC), project ID [GOIPG/2020/971]. The authors would like to thank Novartis (Basel, Switzerland) for supplying siponimod.

References

1 H. Lindekleiv and M. G. Erke, Projected prevalence of age-related macular degeneration in Scandinavia 2012–2040, *Acta Ophthalmol.*, 2013, **91**, 307–311, DOI: **10.1111/j.1755-3768.2012.02399.x**.
2 GBD 2019 Blindness and Vision Impairment Collaborators, Vision Loss Expert Group of the Global Burden of Disease Study, Causes of blindness and vision impairment in 2020 and trends over 30 years, and prevalence of avoidable blindness in relation to VISION 2020: the Right to Sight: an analysis for the Global Burden of Disease Study, *Lancet Global Health*, 2021, **9**, e144–e160, DOI: **10.1016/S2214-109X(20)30489-7**.
3 P. A. Campochiaro, Ocular neovascularization, *J. Mol. Med.*, 2013, **91**, 311–321, DOI: **10.1007/s00109-013-0993-5**.
4 R. A. Alshaikh, C. Waeber and K. B. Ryan, Polymer based sustained drug delivery to the ocular posterior segment: barriers and future opportunities for the treatment of neovascular pathologies, *Adv. Drug Delivery Rev.*, 2022, **187**, 114342, DOI: **10.1016/J.ADDR.2022.114342**.
5 X. Sun, S. Yang and J. Zhao, Resistance to anti-VEGF therapy in neovascular age-related macular degeneration: a comprehensive review, *Drug Des., Dev. Ther.*, 2016, 1857, DOI: **10.2147/DDDT.S97653**.
6 D. Sharma, I. Zachary and H. Jia, Mechanisms of Acquired Resistance to Anti-VEGF Therapy for Neovascular Eye Diseases, *Invest. Ophthalmol. Visual Sci.*, 2023, **64**, 28, DOI: **10.1167/IOVS.64.5.28**.
7 Y. Nakamura, Multiple Therapeutic Applications of RBM-007, an Anti-FGF2 Aptamer, *Cells*, 2021, **10**, 1617, DOI: **10.3390/cells10071617**.

8 X. Ren, J. Li, X. Xu, C. Wang and Y. Cheng, IBI302, a promising candidate for AMD treatment, targeting both the VEGF and complement system with high binding affinity in vitro and effective targeting of the ocular tissue in healthy rhesus monkeys, *Exp. Eye Res.*, 2016, **145**, 352–358, DOI: 10.1016/J.EXER.2016.02.004.

9 Comparison of Age-related Macular Degeneration Treatments Trials (CATT) Research Group, D. F. Martin, M. G. Maguire, S. L. Fine, G. Ying, G. J. Jaffe, J. E. Grunwald, C. Toth, M. Redford and F. L. Ferris, Ranibizumab and bevacizumab for treatment of neovascular age-related macular degeneration: two-year results., *Ophthalmology*, 2012, **119**, 1388–1398, DOI: 10.1016/j.ophtha.2012.03.053.

10 N. Das, S. Chaurasia and R. P. Singh, A review of emerging tyrosine kinase inhibitors as durable treatment of neovascular age-related macular degeneration, *Expert Opin Emerg Drugs*, 2023, **28**, 203–211, DOI: 10.1080/14728214.2023.2259790.

11 C. Niaudet, B. Jung, A. Kuo, S. Swendeman, E. Bull, T. Seno, R. Crocker, Z. Fu, L. E. H. Smith and T. Hla, Therapeutic activation of endothelial sphingosine–1–phosphate receptor 1 by chaperone–bound S1P suppresses proliferative retinal neovascularization, *EMBO Mol. Med.*, 2023, **15**, e16645, DOI: 10.15252/EMMM.202216645.

12 K. Gaengel, C. Niaudet, K. Hagikura, B. L. Siemsen, L. Muhl, J. J. Hofmann, L. Ebarasi, S. Nyström, S. Rymo, L. L. Chen, M. F. Pang, Y. Jin, E. Raschperger, P. Roswall, D. Schulte, R. Benedito, J. Larsson, M. Hellström, J. Fuxe, P. Uhlén, R. Adams, L. Jakobsson, A. Majumdar, D. Vestweber, A. Uv and C. Betsholtz, The Sphingosine-1-Phosphate Receptor S1PR1 Restricts Sprouting Angiogenesis by Regulating the Interplay between VE-Cadherin and VEGFR2, *Dev. Cell*, 2012, **23**, 587–599, DOI: 10.1016/J.DEVCEL.2012.08.005.

13 Y. Liu, Q. Yang, H. Fu, J. Wang, S. Yuan, X. Li, P. Xie, Z. Hu and Q. Liu, Müller glia-derived exosomal miR-9–3p promotes angiogenesis by restricting sphingosine-1-phosphate receptor S1P1 in diabetic retinopathy, *Mol. Ther.–Nucleic Acids*, 2022, **27**, 491–504, DOI: 10.1016/j.omtn.2021.12.019.

14 C. M. Sorenson, M. Farnoodian, S. Wang, Y. S. Song, S. R. Darjatmoko, A. S. Polans and N. Sheibani, Fingolimod (FTY720), a Sphinogosine-1-Phosphate Receptor Agonist, Mitigates Choroidal Endothelial Proangiogenic Properties and Choroidal Neovascularization, *Cells*, 2022, **11**, 969, DOI: 10.3390/CELLS11060969.

15 R. A. Alshaikh, R. G. E. Zaki, R. A. S. El Din, K. B. Ryan and C. Waeber, Siponimod As a Novel Inhibitor of Retinal Angiogenesis: In Vitro and In Vivo Evidence of Therapeutic Efficacy, *J. Pharmacol. Exp. Ther.*, 2023, **386**, 224–241, DOI: 10.1124/jpet.122.001529.

16 R. A. Alshaikh, K. B. Ryan and C. Waeber, Sphingosine 1-phosphate, a potential target in neovascular retinal disease, *Br. J. Ophthalmol.*, 2021, 1–9, DOI: 10.1136/BJOPHTHALMOL-2021-319115.

17 R. A. Alshaikh, R. A. Salah, E. Din, R. Gamal, E. Zaki, C. Waeber and K. B. Ryan, In Vivo Ocular Pharmacokinetics and Toxicity of Siponimod in Albino Rabbits, *Mol. Pharm.*, 2024, **21**, 3310–3320, DOI: 10.1021/ACS.MOLPHARMACEUT.4C00063.

18 E. J. Torres-Martinez, J. M. Cornejo Bravo, A. Serrano Medina, G. L. Pérez González and L. J. Villarreal Gómez, A Summary of Electrospun Nanofibers as Drug Delivery System: Drugs Loaded and Biopolymers Used as Matrices, *Curr Drug Deliv*, 2018, **15**, 1360–1374, DOI: 10.2174/1567201815666180723114326.

19 A. Luraghi, F. Peri and L. Moroni, Electrospinning for drug delivery applications: A review, *J. Controlled Release*, 2021, **334**, 463–484, DOI: 10.1016/j.jconrel.2021.03.033.

20 Y. Wang, B. Qin, G. Xia and S. H. Choi, FDA's Poly (Lactic-Co-Glycolic Acid) Research Program and Regulatory Outcomes, *AAPS J.*, 2021, **23**, 1–7, DOI: 10.1208/s12248-021-00611-y.

21 H. Tsujinaka, J. Fu, J. Shen, Y. Yu, Z. Hafiz, J. Kays, D. McKenzie, D. Cardona, D. Culp, W. Peterson, B. C. Gilger, C. S. Crean, J. Z. Zhang, Y. Kanan, W. Yu, J. L. Cleland, M. Yang, J. Hanes and P. A. Campochiaro, Sustained treatment of retinal vascular diseases with self-aggregating sunitinib microparticles, *Nat. Commun.*, 2020, **11**, 1–13, DOI: 10.1038/s41467-020-14340-x.

22 X. Feng, J. Li, X. Zhang, T. Liu, J. Ding and X. Chen, Electrospun polymer micro/nanofibers as pharmaceutical repositories for healthcare, *J. Controlled Release*, 2019, **302**, 19–41, DOI: 10.1016/j.jconrel.2019.03.020.

23 P. I. Siafaka, E. Özcan Bülbül, A. N. Miliotou, I. D. Karantas, M. E. Okur and N. Üstündağ Okur, Delivering active molecules to the eye; the concept of electrospinning as potent tool for drug delivery systems, *J Drug Deliv Sci Technol*, 2023, **84**, 104565, DOI: 10.1016/J.JDDST.2023.104565.

24 D. Mishra, S. Gade, V. Pathak, L. K. Vora, K. Mcloughlin, R. Medina, R. F. Donnelly and T. Raghu Raj Singh, Ocular application of electrospun materials for drug delivery and cellular therapies, *Drug Discovery Today*, 2023, **28**, 103676, DOI: 10.1016/J.DRUDIS.2023.103676.

25 K. Ghosal, A. Chandra, G. Praveen, S. Snigdha, S. Roy, C. Agatemor, S. Thomas and I. Provaznik, Electrospinning over Solvent Casting: Tuning of Mechanical Properties of Membranes, *Sci. Rep.*, 2018, **8**, 1–9, DOI: 10.1038/s41598-018-23378-3.

26 A. Rohani Shirvan, N. Hemmatinejad, S. H. Bahrami and A. Bashari, A comparison between solvent casting and electrospinning methods for the fabrication of neem extract-containing buccal films, *J. Ind. Text.*, 2022, **51**, 311S–335S, DOI: 10.1177/15280837211027785.

27 S.-F. Chou, D. Carson and K. A. Woodrow, Current strategies for sustaining drug release from electrospun nanofibers, *J. Controlled Release*, 2015, **220**, 584–591, DOI: 10.1016/j.jconrel.2015.09.008.

28 U. Angkawinitwong, S. Awwad, P. T. Khaw, S. Brocchini and G. R. Williams, Electrospun formulations of bevacizumab for sustained release in the eye, *Acta Biomater.*, 2017, **64**, 126–136, DOI: 10.1016/j.actbio.2017.10.015.

29 S. O. L. de Souza, M. C. A. Guerra, L. G. D. Heneine, C. R. de Oliveira, A. da, S. Cunha Junior, S. L. Fialho and R. L. Oréfice, Biodegradable core-shell electrospun nanofibers containing bevacizumab to treat age-related macular degeneration, *J. Mater. Sci. Mater. Med.*, 2018, **29**, 173, DOI: 10.1007/s10856-018-6187-5.

30 M. C. A. Guerra, J. T. Neto, M. G. Gomes, L. F. N. Dourado, R. L. Oréfice, L. G. D. Heneine, A. Silva-Cunha and S. L. Fialho, Nanofiber-coated implants: Development and safety after intravitreal application in rabbits, *Int. J. Pharm.*, 2023, **636**, 122809, DOI: 10.1016/j.ijpharm.2023.122809.

31 I. A. Khalil, I. H. Ali and I. M. El-Sherbiny, Noninvasive Biodegradable Nanoparticles-in-Nanofibers Single-Dose Ocular Insert: In Vitro, Ex Vivo and In Vivo Evaluation, *Nanomedicine*, 2019, **14**, 33–55, DOI: 10.2217/nnm-2018-0297.

32 R. Qi, R. Guo, M. Shen, X. Cao, L. Zhang, J. Xu, J. Yu and X. Shi, Electrospun poly(lactic-co-glycolic acid)/halloysite nanotube composite nanofibers for drug encapsulation and sustained release, *J. Mater. Chem.*, 2010, **20**, 10622, DOI: 10.1039/c0jm01328e.

33 ICH Topic Q 2 (R1) Validation of Analytical Procedures: Text and Methodology Step 5 NOTE FOR GUIDANCE ON VALIDATION OF ANALYTICAL PROCEDURES: TEXT AND METHODOLOGY (CPMP/ICH/381/95) APPROVAL BY CPMP November 1994 DATE FOR COMING INTO OPERATION,1995. https://www.emea.eu.int(accessed June 21, 2023).

34 B. G. Amsden and D. Marecak, Long-term sustained release from a biodegradable photo-cross-linked network for intraocular corticosteroid delivery, *Mol. Pharm.*, 2016, **13**, 3004–3012, DOI: 10.1021/acs.molpharmaceut.6b00358.

35 H. K. Makadia and S. J. Siegel, Poly Lactic-co-Glycolic Acid (PLGA) as Biodegradable Controlled Drug Delivery Carrier, *Polymers*, 2011, **3**, 1377, DOI: 10.3390/POLYM3031377.

36 I. M. Hodge, Physical Aging in Polymer Glasses, *Science*, 1979, **267**(1995), 1945–1947, DOI: 10.1126/science.267.5206.1945.

37 Z. Sartawi, C. Waeber, E. Schipani and K. B. Ryan, Development of electrospun polymer scaffolds for the localized and controlled delivery of siponimod for the management of critical bone defects, *Int. J. Pharm.*, 2020, **590**, 119956, DOI: 10.1016/j.ijpharm.2020.119956.

38 A. Haider, K. C. Gupta and I.-K. Kang, Morphological Effects of HA on the Cell Compatibility of Electrospun HA/PLGA Composite Nanofiber Scaffolds, *BioMed Res. Int.*, 2014, **2014**, 1–11, DOI: 10.1155/2014/308306.

39 R. A. Alshaikh, E. A. Essa and G. M. El Maghraby, Eutexia for enhanced dissolution rate and anti-inflammatory activity of nonsteroidal anti-inflammatory agents: Caffeine as a melting point modulator, *Int. J. Pharm.*, 2019, **563**, 395–405, DOI: 10.1016/j.ijpharm.2019.04.024.

40 V. Arjunan, C. V. Mythili, K. Mageswari and S. Mohan, Experimental and theoretical investigations of benzamide oxime, *Spectrochim. Acta, Part A*, 2011, **79**, 245–253, DOI: 10.1016/j.saa.2011.02.050.

41 L. Kappos, D. K. B. Li, O. Stöve, H. P. Hartung, M. S. Freedman, B. Hemmer, P. Rieckmann, X. Montalban, T. Ziemssen, B. Hunter, S. Arnould, E. Wallström and K. Selmaj, Safety and Efficacy of Siponimod (BAF312) in Patients With Relapsing-Remitting Multiple Sclerosis: Dose-Blinded, Randomized Extension of the Phase 2 BOLD Study, *JAMA Neurol.*, 2016, **73**, 1089–1098, DOI: 10.1001/JAMANEUROL.2016.1451.

42 S. Dash, P. N. Murthy, L. Nath and P. Chowdhury, Kinetic modeling on drug release from controlled drug delivery systems, *Acta Pol. Pharm.*, 2010, **67**, 217–223.

43 J. Siepmann and N. A. Peppas, Modeling of drug release from delivery systems based on hydroxypropyl methylcellulose (HPMC), *Adv. Drug Delivery Rev.*, 2012, **64**, 163–174, DOI: 10.1016/j.addr.2012.09.028.

44 R. L. Vincelette, A. J. Welch, R. J. Thomas, B. A. Rockwell and D. J. Lund, Thermal lensing in ocular media exposed to continuous-wave near-infrared radiation: the 1150–1350 nm region, *J. Biomed. Opt.*, 2008, **13**, 054005, DOI: 10.1117/1.2978066.

45 M. G. McKee, G. L. Wilkes, R. H. Colby and T. E. Long, Correlations of Solution Rheology with Electrospun Fiber Formation of Linear and Branched Polyesters, *Macromolecules*, 2004, **37**, 1760–1767, DOI: 10.1021/ma035689h.

46 R. Casasola, N. L. Thomas, A. Trybala and S. Georgiadou, Electrospun poly lactic acid (PLA) fibres: Effect of different solvent systems on fibre morphology and diameter, *Polymer*, 2014, **55**, 4728–4737, DOI: 10.1016/j.polymer.2014.06.032.

47 J. Xie and C.-H. Wang, Electrospun Micro- and Nanofibers for Sustained Delivery of Paclitaxel to Treat C6 Glioma in Vitro, *Pharm. Res.*, 2006, **23**, 1817–1826, DOI: 10.1007/s11095-006-9036-z.

48 I. Krucińska, M. Boguń, O. Chrzanowska, M. Chrzanowski and P. Król, Research concerning fabrication of fibrous osteoconductive plga/hap nanocomposite material using the method of electrospinning from polymer solution, *Autex Res. J.*, 2013, **13**, 57–66, DOI: 10.2478/v10304-012-0027-3.

49 J. Xie, X. Li and Y. Xia, Putting Electrospun Nanofibers to Work for Biomedical Research., *Macromol. Rapid Commun.*, 2008, **29**, 1775–1792, DOI: 10.1002/marc.200800381.

50 F. Zamani, M. Amani-Tehran, M. Latifi and M. A. Shokrgozar, The influence of surface nanoroughness of electrospun PLGA nanofibrous scaffold on nerve cell adhesion and proliferation, *J. Mater. Sci. Mater. Med.*, 2013, **24**, 1551–1560, DOI: 10.1007/s10856-013-4905-6.

51 S. Megelski, J. S. Stephens, D. B. Chase and J. F. Rabolt, Micro- and Nanostructured Surface Morphology on Electrospun Polymer Fibers, *Macromolecules*, 2002, **35**, 8456–8466, DOI: 10.1021/ma020444a.

52 R. M. Nezarati, M. B. Eifert and E. Cosgriff-Hernandez, Effects of Humidity and Solution Viscosity on Electrospun Fiber Morphology, *Tissue Eng., Part C*, 2013, **19**, 810–819, DOI: 10.1089/ten.tec.2012.0671.

53 M. Ranjbar-Mohammadi, M. Zamani, M. P. Prabhakaran, S. H. Bahrami and S. Ramakrishna, Electrospinning of PLGA/gum tragacanth nanofibers containing tetracycline hydrochloride for periodontal regeneration, *Mater. Sci. Eng., C*, 2016, **58**, 521–531, DOI: 10.1016/j.msec.2015.08.066.

54 M. Abou-ElNour, R. A. H. Ishak, M. Tiboni, G. Bonacucina, M. Cespi, L. Casettari, M. E. Soliman and A. S. Geneidi, Triamcinolone acetonide-loaded PLA/PEG-PDL microparticles for effective intra-articular delivery: synthesis, optimization, in vitro and in vivo evaluation, *J. Controlled Release*, 2019, **309**, 125–144, DOI: 10.1016/J.JCONREL.2019.07.030.

55 G. Jiang, H. Jia, J. Qiu, Z. Mo, Y. Wen, Y. Zhang, Y. Wen, Q. Xie, J. Ban, Z. Lu, Y. Chen, H. Wu, Q. Ni, F. Chen, J. Lu, Z. Wang, H. Li and J. Chen, PLGA Nanoparticle Platform for Trans-Ocular Barrier to Enhance Drug Delivery: A Comparative Study Based on the Application of Oligosaccharides in the Outer Membrane of Carriers, *Int. J. Nanomed.*, 2020, **15**, 9373–9387, DOI: 10.2147/IJN.S272750.

56 P. Taepaiboon, U. Rungsardthong and P. Supaphol, Drug-loaded electrospun mats of poly(vinyl alcohol) fibres and their release characteristics of four model drugs, *Nanotechnology*, 2006, **17**, 2317–2329, DOI: 10.1088/0957-4484/17/9/041.

57 S. M. Jusu, J. D. Obayemi, A. A. Salifu, C. C. Nwazojie, V. Uzonwanne, O. S. Odusanya and W. O. Soboyejo, Drug-encapsulated blend of PLGA-PEG microspheres: in vitro and in vivo study of the effects of localized/targeted drug delivery on the treatment of triple-negative breast cancer, *Sci. Rep.*, 2020, **10**, 1–23, DOI: 10.1038/s41598-020-71129-0.

58 S. F. Chou and K. A. Woodrow, Relationships between mechanical properties and drug release from electrospun fibers of PCL and PLGA blends, *J. Mech. Behav. Biomed. Mater.*, 2017, **65**, 724–733, DOI: 10.1016/J.JMBBM.2016.09.004.

59 Y. Xu, C. Kim, D. M. Saylor and D. Koo, Polymer degradation and drug delivery in PLGA–based drug–polymer applications: A review of experiments and theories, *J. Biomed. Mater. Res., Part B*, 2017, **105**, 1692–1716, DOI: 10.1002/jbm.b.33648.

60 N. S. Heredia, K. Vizuete, M. Flores-Calero, K. Pazmiño, V. F. Pilaquinga, B. Kumar and A. Debut, Comparative statistical analysis of the release kinetics models for nanoprecipitated drug delivery systems based on poly(lactic-co-glycolic acid), *PLoS One*, 2022, **17**, e0264825, DOI: 10.1371/journal.pone.0264825.

61 P. Costa and J. M. Sousa Lobo, Modeling and comparison of dissolution profiles, *Eur. J. Pharm. Sci.*, 2001, **13**, 123–133, DOI: 10.1016/S0928-0987(01)00095-1.

62 T. Higuchi, Rate of Release of Medicaments from Ointment Bases Containing Drugs in Suspension, *J. Pharm. Sci.*, 1961, **50**, 874–875, DOI: 10.1002/JPS.2600501018.

63 S. Fredenberg, M. Wahlgren, M. Reslow and A. Axelsson, The mechanisms of drug release in poly(lactic-co-glycolic acid)-based drug delivery systems—A review, *Int. J. Pharm.*, 2011, **415**, 34–52, DOI: 10.1016/j.ijpharm.2011.05.049.

64 H. K. Kim and T. G. Park, Comparative study on sustained release of human growth hormone from semi-crystalline poly(l-lactic acid) and amorphous poly(d,l-lactic-co-glycolic acid) microspheres: morphological effect on protein release, *J. Controlled Release*, 2004, **98**, 115–125, DOI: 10.1016/j.jconrel.2004.04.020.

65 L. Y. Lee, S. H. Ranganath, Y. Fu, J. L. Zheng, H. S. Lee, C.-H. Wang and K. A. Smith, Paclitaxel release from microporous PLGA disks, *Chem. Eng. Sci.*, 2009, **64**, 4341–4349, DOI: 10.1016/j.ces.2009.07.016.

66 T. T. T. Nguyen, C. Ghosh, S.-G. Hwang, N. Chanunpanich and J. S. Park, Porous core/sheath composite nanofibers fabricated by coaxial electrospinning as a potential mat for drug release system, *Int. J. Pharm.*, 2012, **439**, 296–306, DOI: 10.1016/j.ijpharm.2012.09.019.

67 F. Ajalloueian, H. Tavanai, J. Hilborn, O. Donzel-Gargand, K. Leifer, A. Wickham and A. Arpanaei, Emulsion Electrospinning as an Approach to Fabricate PLGA/Chitosan Nanofibers for Biomedical Applications, *BioMed Res. Int.*, 2014, **2014**, 475280, DOI: 10.1155/2014/475280.

68 A. N. Lembach, H. B. Tan, I. V. Roisman, T. Gambaryan-Roisman, Y. Zhang, C. Tropea and A. L. Yarin, Drop impact, spreading, splashing, and penetration into electrospun nanofiber mats, *Langmuir*, 2010, **26**, 9516–9523, DOI: 10.1021/la100031d.

69 A. Clarke, T. D. Blake, K. Carruthers and A. Woodward, Spreading and imbibition of liquid droplets on porous surfaces, *Langmuir*, 2002, **18**, 2980–2984.

70 D. Carson, Y. Jiang and K. A. Woodrow, Tunable Release of Multiclass Anti-HIV Drugs that are Water-Soluble and Loaded at High Drug Content in Polyester Blended Electrospun Fibers, *Pharm. Res.*, 2016, **33**, 125–136, DOI: 10.1007/s11095-015-1769-0.

71 B. Duan, L. Wu, X. Li, X. Yuan, X. Li, Y. Zhang and K. Yao, Degradation of electrospun PLGA-chitosan/PVA membranes and their cytocompatibility in vitro, *J. Biomater. Sci., Polym. Ed.*, 2007, **18**, 95–115, DOI: 10.1163/156856207779146105.

72 K. A. Blackwood, R. McKean, I. Canton, C. O. Freeman, K. L. Franklin, D. Cole, I. Brook, P. Farthing, S. Rimmer, J. W. Haycock, A. J. Ryan and S. MacNeil, Development of biodegradable electrospun scaffolds for dermal replacement, *Biomaterials*, 2008, **29**, 3091–3104, DOI: 10.1016/j.biomaterials.2008.03.037.

73 S. Li, S. Girod-Holland and M. Vert, Hydrolytic degradation of poly(dl-lactic acid) in the presence of caffeine base, *J. Controlled Release*, 1996, **40**, 41–53, DOI: 10.1016/0168-3659(95)00138-7.

74 S. Siegel, J. Kahn, K. Metzger, K. Winey, K. Werner and N. Dan, Effect of drug type on the degradation rate of PLGA matrices, *Eur. J. Pharm. Biopharm.*, 2006, **64**, 287–293, DOI: 10.1016/j.ejpb.2006.06.009.

75 C. L. Huang, T. W. Steele, E. Widjaja, F. Y. Boey, S. S. Venkatraman and J. S. Loo, The influence of additives in modulating drug delivery and degradation of PLGA thin films, *NPG Asia Mater.*, 2013, **5**, e54–e54, DOI: 10.1038/am.2013.26.

76 G. Van den Mooter, M. Wuyts, N. Blaton, R. Busson, P. Grobet, P. Augustijns and R. Kinget, Physical stabilis-

ation of amorphous ketoconazole in solid dispersions with polyvinylpyrrolidone K25, *Eur. J. Pharm. Sci.*, 2001, **12**, 261–269, DOI: **10.1016/S0928-0987(00)00173-1**.

77 K. J. Crowley and G. Zografi, The effect of low concentrations of molecularly dispersed poly(vinylpyrrolidone) on indomethacin crystallization from the amorphous state., *Pharm. Res.*, 2003, **20**, 1417–1422, DOI: **10.1023/a:1025706110520**.

78 C. Bhugra and M. J. Pikal, Role of Thermodynamic, Molecular, and Kinetic Factors in Crystallization from the Amorphous State, *J. Pharm. Sci.*, 2008, **97**, 1329–1349, DOI: **10.1002/JPS.21138**.

79 F. Theil, J. Milsmann, S. O. Kyerematen, S. Anantharaman, J. Rosenberg and H. van Lishaut, Extraordinary Long-Term-Stability in Kinetically Stabilized Amorphous Solid Dispersions of Fenofibrate, *Mol. Pharm.*, 2017, **14**, 4636–4647, DOI: **10.1021/acs.molpharmaceut.7b00735**.

80 F. Theil, S. Anantharaman, S. O. Kyerematen, H. van Lishaut, S. H. Dreis-Kühne, J. Rosenberg, M. Mägerlein and G. H. Woehrle, Frozen in Time: Kinetically Stabilized Amorphous Solid Dispersions of Nifedipine Stable after a Quarter Century of Storage, *Mol. Pharm.*, 2017, **14**, 183–192, DOI: **10.1021/acs.molpharmaceut.6b00783**.